TOWARDS THE DESIGN OF ULTRASOUND CONTRAST AGENTS: INVESTIGATION OF MONOLAYER MICROSTRUCTURE

A Thesis Submitted to
the Graduate School of Engineering and Sciences of
İzmir Institute of Technology
in Partial Fulfillment of the Requirements for the Degree of

MASTER OF SCIENCE

in Biotechnology

by
Saliha Zeyneb AKINCI

July, 2011
İZMİR

We approve the thesis of **Saliha Zeyneb AKINCI**

_____

Assist. Prof. Dr. Sevgi KILIÇ ÖZDEMİR
Supervisor

_____

Prof. Dr. Serdar ÖZÇELİK
Co-Advisor

_____

Prof. Dr. Mehmet POLAT
Committee Member

_____

Assist. Prof. Dr. Yusuf SELAMET
Committee Member

_____

Assist. Prof. Dr. Hadi M. ZAREIE
Committee Member

4 July 2011

_____

Assoc. Prof. Dr. Volga BULMUŞ
Head of the Department of
Biotechnology and Bioengineering

_____

Prof. Dr. Durmuş Ali DEMİR
Dean of the Graduate School of
Engineering and Sciences

ACKNOWLEDGEMENTS

I thank my supervisor Assist. Prof. Dr. Sevgi KILIÇ ÖZDEMİR for her invaluable support and knowledge that she provided to me during my study.

Also, I thank Prof. Dr. Serdar ÖZÇELİK for his invaluable comments and encouragements that made me motivated throughout my studies.

Moreover, I want to thank Assist. Prof. Dr. Hadi M. ZAREIE for his positive attitudes and helpfullness whenever I ask him questions in the lab. I will never forget his encouragements during my studies.

I am also thankful TUBITAK for providig me project funding (TUBITAK-MAG) for 4,5 months between 15th April 2010 and 30th August 2010.

My special thanks go to my parents and my brother, for being always with me with their endless support and love and also encourage me to go further in science.

Also, I am deeply appreciated my relatives for their motivation, love and precious prayers in all parts of my life since I was born. Thank you again. Besides, I thank God, for allowing me to overcome this struggling but thoughtful stage of my life.

ABSTRACT

TOWARDS THE DESIGN OF ULTRASOUND CONTRAST AGENTS: INVESTIGATION OF MONOLAYER MICROSTRUCTURE

This thesis work is focused on the monolayer formation of phospholipid molecules and surfactants by Langmuir-Blodgett thin film technique on air/water or phosphate buffer interfaces. This study is also devoted to find out the effect of surfactants, the mixing ratio of the components, and also the phosphate buffer solutions on the monolayer films. The pH of the phosphate buffer solution that is used in experiments, is 7.2 and is coherent with the human blood plasma.

In addition to this technique, a microscopic technique is employed. The monolayer features in different liquid interfaces are investigated by Brewster angle microscopy technique.

In this study, the effect of ionic strength coming from the buffer solutions are examined in whole pure components and mixtures. It is aimed to find out to obtain more detailed information from the surface-pressure versus mean molecular area isotherms that are obtained from Langmuir-Blodgett technique. Therefore, the exact behavior of these organic thin films at the air/liquid interfaces are studied.

The miscibility behavior and thermodynamic analysis of the mixed monolayers are also examined for each of the mixtures.

ÖZET

ULTRASON KONTRAST AJANLARININ TASARIMINA DOĞRU: MONOTABAKANIN MİKROYAPISININ İNCELENMESİ

Bu tez çalışması, Langmuir-Blodgett ince film tekniği ile surfaktan ve fosfolipid moleküllerinin saf su ve fosfat çözeltisi yüzeylerindeki tek tabakalı yüzey oluşumuna odaklanmıştır. Bu çalışma, ayrıca surfaktant moleküllerin, saf moleküllerin oluşturdukları karışımların ve de fosfat çözeltilerin tek tabakalı yüzeydeki etkilerini bulmaya adanmıştır. Deneylerde kullanılan fosfat çözeltilerinin pH değeri 7.2 olup, insan kanının pH değeri ile uyumludur.

Bu tekniğe ek olarak, bir mikroskopik teknik de kullanılmıştır. Farklı sıvı yüzeylerindeki tek tabakalı yüzey özellikleri, Brewster açı mikroskobu tekniği ile araştırılmıştır.

Bu çalışmada, fosfat çözeltilerinden kaynaklanan iyonik etki bütün saf moleküllerde ve karışımlarda incelenmiştir. Langmuir-Blodgett tekniği ile elde edilen yüzey basıncına karşı ortalama moleküler alan izotermlerinden daha detaylı bilgi elde etmek amaçlanmıştır. Sonuç olarak, bu organik ince filmlerin sıvı/hava ara yüzeylerindeki gerçek davranışları çalışılmıştır.

Karışımlardan oluşan tek tabakalı yüzeylerin birbirlerine karışabilme davranışları ve termodinamik analizleri de her çözelti için incelenmiştir.

I dedicated this thesis to all my family members,

for their endless support and encouragement

in all parts of my life.

TABLE OF CONTENTS

LIST OF FIGURES

Figure **Page**

LIST OF TABLES

Table **Page**

CHAPTER 1

INTRODUCTION

In medical imaging, especially in therapeutic purposes, ultrasound is the most commonly used one (Unger et al., 2004). Because among other imaging techniques, such as X-ray radiology and magnetic resonance imaging, it has many benefits. In addition to its real-time imaging quality, it is also cheap, portable and non-invasive (Riess et al., 2003; Liang and Blomley, 2003; Klibanov, 2005).

In spite of these advantages, ultrasound needs effective contrast agents in order to enhance the image quality. These special agents, which are known as ideal reflectors of ultrasound at a diagnostic frequency, are micron-sized gas bubbles (Riess et al., 2003). Microbubbles, which are encapsulated by a surfactant shell, have diameters between 0.1-100 micrometers. They are being used in many biomedical areas including ultrasound imaging as contrast agents and therapeutic applications as delivery vehicles in targeting purposes (Borden, 2009).

Micron-sized gas bubbles which are injected intraveneously cannot keep their stability through circulation. The gas part of them diffuses out through the shells and passes through the biological fluids in the body and then exhaled through lungs (Klibanov, 2005). The interaction between the ultrasound and the microbubbles increase the image quality. The sound waves propagates more slowly in the gaseous atmospheres then in liquid ones. This difference results in an acoustic impedance between the blood around the microbubble and the surrounding tissues (Unger et al., 2004).

The coating part of the microbubbles may be consisted of surfactants, lipids, proteins or polymers. Among these shell materials, lipid-coated microbubbles are the most commonly used ones because of their advantages. Phospholipid molecules allow to obtain highly ordered monolayer film at the air/water interface. Their hydrophobic acyl chains direct to the gaseous part and also hydrophilic head group of them face the aqueous part. Additionally, because of the hydrophobic and Van der Waals interactions between acyl chains, lipid monolayer shells provide high cohesion (Sirsi and Borden, 2009).

The monolayer shell of a microbubble is commonly formed with a main phospholipid component as DinPC and polyethylene glycol 40 stearate (PEG 40 S) (Pu et al., 2006). The investigation of the stable microbubbles offer to use the Langmuir-Blodgett (LB) technique for the nanostructural features of them, especially in high compression rates and also in the specific regions where curvature effects are important (Borden, 2009).

According to the study of Hollinshead and his co-workers investigated the monolayer structure of DSPC by using the LB, Brewster angle microscopy (BAM) and neutron reflectivity techniques. According to the BAM images at the air/water interface, there is not a heterogeneous domain formation. DSPC forms homogeneous phosholipid structure on the subphase (Hollinshead et al., 2009).

The study of Pu and his co-workers also employed LB technique for the surface pressure-area events of the phospholipids in two dimension. Also, they used fluorescence microscopy to observe the effects directly on the shell structure. Microbubbles demonstrated two-phase separation between DinPC and the emulsifier, PEG 40 S (Pu et al., 2006).

In another study, Borden and Longo studied the dissolution behavior of lipid-coated microbubbles and also investigated the shell phase formation with different acyl chain lengths (DinPC, n=12, 14, 16, 18, 20, 22 and 24). The spherical form of the microbubbles was dissapeared when n was increased. The deformed spherical shape had more smaller size (Borden and Longo, 2002; Longo et al., 2004).

The stability of microbubbles is a really important problem after intravenous injection and also in storage. Therefore, the stability of the encapsulated shells should be improved in order to decrease the diffusion of gaseous molecules through the outer part of the bubbles (Riess et al., 2003).

The aim of this thesis study is to investigate the shell sturcture of microbubbles, which includes surfactant-phospholipid interactions at the air/water or at interfaces for different ionic strength conditions by the LB technique. Also, it is intended to visualize the monolayer phases with the BAM technique on the liquid interfaces.

Thesis includes six chapters. Chapter 2 is the literature review of ultrasound contrast agents as microbubbles. Chapter 3 gives a brief information of LB technique. Chapter 4 gives the experimental methods used in the studies and also the procedures for buffer preparations. Chapter 5 is devoted to the results and discussions part and the last chapter gives the conclusive remarks and summaries of the analysis and results.

CHAPTER 2

LITERATURE REVIEW: MICROBUBBLES AS ULTRASOUND CONTRAST AGENTS

2.1. The Discovery of Ultrasound Contrast Agents

The discovery of ultrasound contrast agents in the late 1960's was an accident done by Dr. Claude Joyner. After an injection of indocyanine green dye to the patient's left ventricule for echocardiography, the ultrasound signal increased immediately. He thought that this temporary increase in the contrast was because of the dye. For that reason, he tried several other fluids, including saline (Stride and Edisiringhe, 2008).

In 1968, Gramiak and Shah proposed that this contrast effect was coming from the air bubbles in the blood vessels. After increasing the ambient pressure, no contrast enhancement was observed. Therefore, this experiment proved the validity of this theory (Gramiak and Shah, 1968; reviwed in Stride and Edisiringhe, 2008; reviewed in Klibanov, 2005; reviewed in Riess et al., 2003; reviewed in Dijkmans et al., 2004).

After this discovery, ultrasound contrast agents were considered to be used in clinical applications. However, the stability, in other words, the life time of the microbubbles, which were formed during the injection of dye or saline, was not so effective under high surface tension, they dissolve quickly. The other important point was related with their size. Their diameters exceeded the capillary bed (Riess et al., 2003). Thus, imaging the left ventricular of the heart was impossible. Since they were unstable in the blood vessels, it was considered that an encapsulated shell formation for the gas bubbles could provide stability for echogenicity (Riess et al., 2003). For this reason, it was thought that mixing the microbubble suspension with the blood could be improve the stability. The first generated ones were composed of air, but the air-filled microbubbles disappeared quickly in vivo since the solubility of the air in the human blood was high (Dijkmans et al., 2004).

The first commercial microbubbles (Table 2.1) with albumin-coated shells were developed with this idea under the trade name of Albunex. Several agents were approved by the FDA in Europe after the production of Albunex. One of them was

Levovist (Stride and Edisiringhe, 2008). This agent was also developed to improve the stability and the contained galactose palmitic acid. These bubbles could pass through the capillary bed. However, since the pressure in the arteries were strong, they could not resist that force (Dijkmans et al., 2004).

Table 2.1. The microbubbles currently available or under commercial development (Source: Stride and Edisiringhe, 2008)

Name(s)	Manufacturer	Stabilising coating	Filling gas
SonoVue®	Bracco Diagnostics, Inc.	Phospholipid	Sulfur hexafluoride
Definity®	Bristol-Myers Squibb	Phospholipid	Octafluoropropane
Aerosomes™	Medical Imaging Inc.		
MRX115			
DMP115			
Optison™	Amersham Health plc. (GE-Healthcare Inc.)	Cross-linked human serum-albumin	Octafluoropropane
Filmix™	Cav-Con Inc.	Phospholipid	Air
Imavist™	Alliance Pharmaceutical-Corp. Schering AG	Surfactant	Perfluorohexane and air
Imagent®			
Albunex®	Molecular Biosystems-(Mallinckrodt Inc.)	Sonicated human serum-albumin	Air
Sonazoid™	Amersham Health plc. (GE-Healthcare Inc.)	Phospholipid	Perfluorocarbon
Bisphere™	Point Biomedical Corp.	Polymer–protein bilayer	Air
Quantison™	Quadrant Healthcare plc.	Spray dried serum albumin	Air
Echovist®	Schering AG	None	Air
Levovist®	Schering AG	Palmitic acid	Air
Sonavist™	Schering AG	Cyanoacrylate	Air
SHU 563 A			
Echogen®	Sonus Pharmaceuticals Inc.	Surfactant	Dodecafluoropentane

The next generation of microbubbles was produced using high molecular weight gases like sulphur hexafluoride and perfluorocarbon (PFC) in order to decrease the solubility of the bubbles. Sonovue, which was used in diagnostic imaging, was a second-generation microbubble with a phospholipid outer layer around a sulphur hexafluoride gas (Dijkmans et al., 2004).

Following this type, low solubility gases like perfluorocarbon (PFC), was used in the formulation of Optison microbubbles and these were approved by the US FDA for contrast echocardiography (Sirsi and Borden, 2009). PFC gases have low solubility properties and also have been used in the current ultrasound contrast agent products for the stabilization of gas bubbles after the intraveneous injection. These high molecular weight gases are not metabolized in the human body. However, the gaseous part can be exhaled through the lungs when injected intravenously (Riess et al., 2003).

Figure 2.1 shows the osmotically stabilized microbubble after injection. This osmotic equilibrium is constructed between the gases with the partial pressure of 1 atm through the shell part of the microbubble. When PFC gas is added in addition to these gases, a balance is set up between blood and Laplace pressures (Riess et al., 2003).

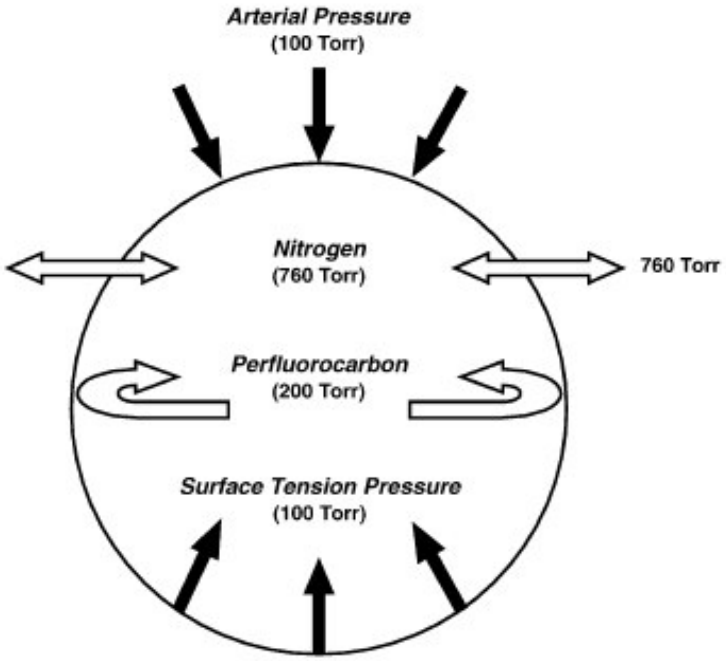

Figure 2.1. The forces acting on the microbubble after intraveneous injection.
(Source: Riess et al., 2003)

2.2. The Structure of Microbubbles

The production of a microbubble is like the enclosed shape of a Langmuir monolayer which encapsulates the gaseous phase with the surfactant molecules on the water surface (Borden, 2009).

An ultrasound contrast agent which allows to differentiate between different tissues like normal and diseased ones, provides distinct backscatter echoes. Thus, the acoustic impedance, which is known as the resistance to sound propagation, is different between these tissues. Additionally, microbubbles under the effect of ultrasound waves, resonate and increase the backcatter echoes more than red blood cells (Riess et al., 2003).

Generally, the microbubbles have a diameter range between 0.5-10 μm in biomedical applications. The diameter must not exceed that limit since they can not pass through the lung capillaries (Sirsi and Borden, 2009).

An ideal contrast agent should be highly echogenic and also have small diameters so as to pass through the pulmonary, cardiac and capillary circulations. In addition, they should be stable for about 6 months in certain conditions and also should be kept in the body for at least 10 minutes. Moreover, they should be injectable intravenously and should be non-toxic (Riess et al., 2003).

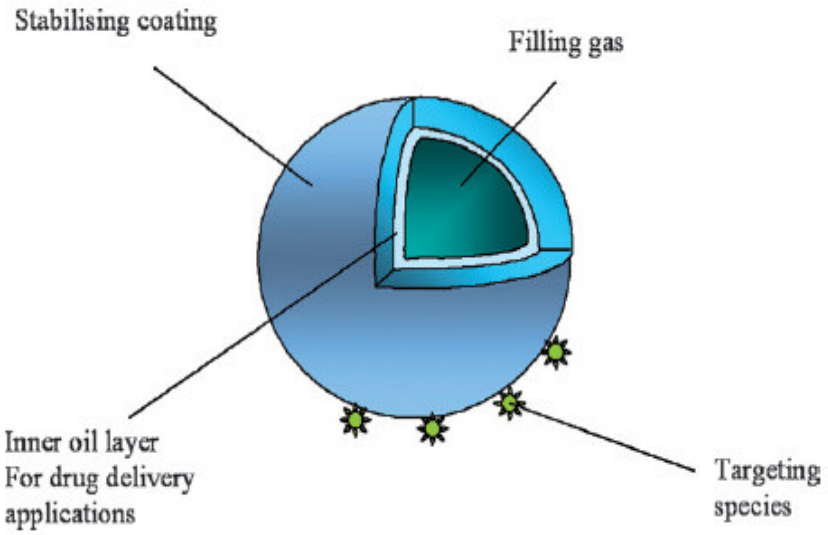

Figure 2.2. The illustration of a microbubble
(Source: Stride and Edisiringhe, 2008)

Ultrasound imaging is very well distributed with gas-based contrast agents through the enhanced backscattered signal intensity. Thus, they can provide high quality images in clinical applications by the detection of cardiovascular abnormalities and solid organ wounds, such as tumors (Figure 2.3) in the body. Moreover, early and accurate detection of diseases can be achievable with the injection of microbubbles (Riess et al., 2003).

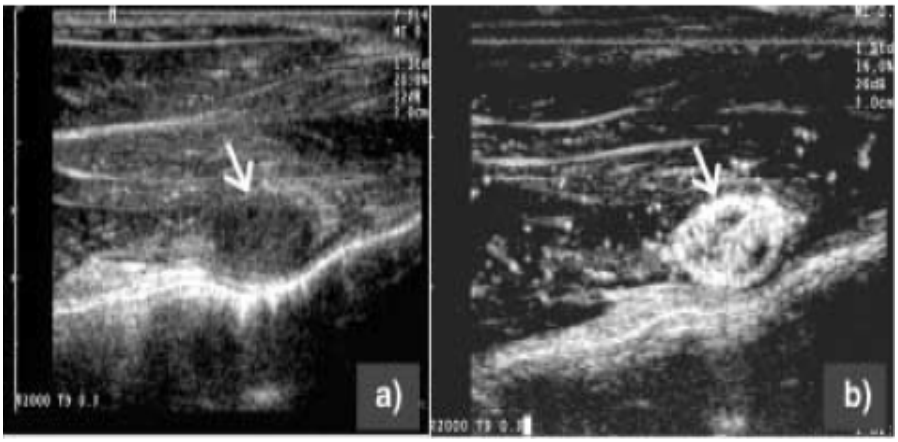

Figure 2.3. Image of a tumor of a rabbit before (a) and after (b) intravenous injection of microbubbles. (Source: Riess et al., 2003)

Moreover, microbubbles are considered as the new generation of drug and gene delivery vehicles since they have promising properties such as their acoustic properties. During the compression phase, the gas core of the microbubble expands and contracts under the pressure of the ultrasound wave (Sirsi and Borden, 2009). The acoustic pressure used in the diagnostic imaging with contrast agents is higher than 0.05 mechanical index. However, acccording to the destruction-reperfusion technique,higher mechanical index (MI) pulses might destruct the imaging area where the microbubble contrast agents are injected intraveneously (Sboros and Tang, 2010). The signal-noise ratio is enhanced in harmonic imaging modality by transmitting the main frequency and receiving multiples of this frequency. As a result of this acoustic impedance mismatch, use of microbubbles in diagnostic ultrasonic imaging is very beneficial. Linear and non-linear oscillations are observed in acoustic pressures. Additionally, high pressure ultrasound signal with the mechanical index of 1 results in microbubble expansion, compression and destruction (Dijkmans et al., 2004).

2.3. Types of Microbubbles

In order to improve the stabilization of micron-sized gas bubbles, sonicated albumin-molecules, surfactants, polymers, and also phospholipids are used. Each of these types has special advantages and functions (Borden et al., 2005; Sirsi and Borden 2009; Dijkmans et al., 2004). Figure 2.2 is the representation of a microbubble.

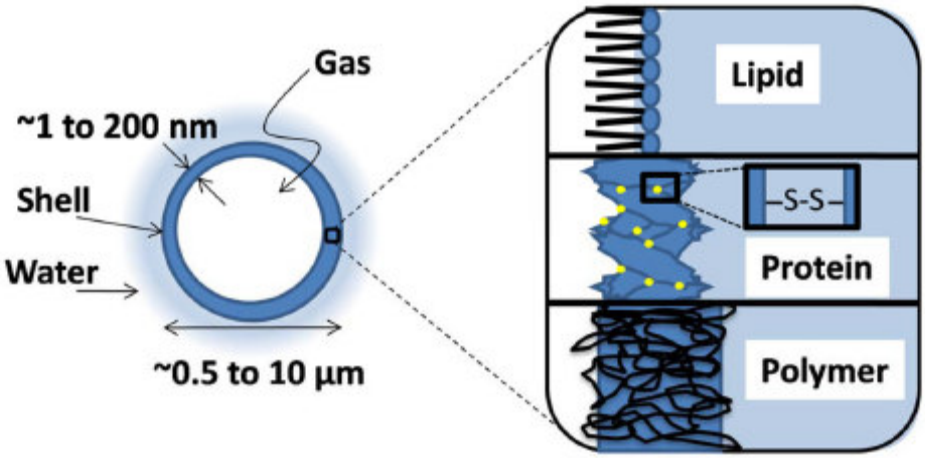

Figure 2.4. The representation of a typical microbubble with different shell components. (Source: Sirsi and Borden, 2008)

2.3.1. Albumin-Coated Microbubbles

The first generated microbubbles began with the albumin-coated ones. They were used in ultrasound contrast imaging, especially in the imaging of left ventricular of the heart (Stride and Edisiringhe, 2008). Albunex was the first albumin-coated microbubble that was approved by the US Food and Drug Administration (FDA). The size of the Albunex microbubble differed from 1-15 micrometers in diameter and they kept their stability in refrigarator for at least two years (Stride and Edisiringhe, 2008).

As a result of the sonication of a heated solution of human serum albumin in air, microbubbles which were encapsulated by a thick shell about 15 nm, were obtained. Heating was very important in order to denature the albumin before the sonication and also facilitated the encapsulation process. The monolayer albumin shell of microbubbles had an interaction between cystein residues that were formed during cavitation. Disulfide bonds between cystein residues, which were formed during cavitation, were dominant through the monolayer albumin shell of microbubbles. Because of the covalent cross-linking interaction, the albumin-coated shells were so rigid under ultrasound (Sirsi and Borden, 2009) and resulted in poor image quality. Moreover, albumin-coated microbubbles adhere to the endothelial cells, preventing their free ciculation in the blood stream (Unger et al., 2004).

2.3.2. Surfactant-Coated Microbubbles

Wang et al. investigated that the surfactant air microbubbles, which were produced by sonication methods, so as to obtain their stable formation. Langmuir-Blodgett technique was employed in order to determine the correct ratio of surfactant (Span/Tween) molecules. They found that the sonicated solution of microbubbles indicated more stability after spreading the solution on the Langmuir trough. The related isotherm of this experiment showed that high collapse pressure values were obtained (Wang et al., 1996).

2.3.3. Polymer-Coated Microbubbles

The shell behavior of protein or polymer-coted microbubbles was investigated with optical and acoustical methods. These type of coating resulted in cracks and disruption of the monolayer shell. Also, the echogenicity was decreased in the use of polymer-coated microbubbles (Borden et al., 2005).

It was thought that the polymer-coated microbubbles could resist to the pressure more than the other coating materials. These type of microbubbles provided thicker and more stable agents, but they were resistant to ultrasound. The polymeric shell decreased the efficiency of the ultrasound waves (Riess et al., 2003). Polymer-coated microbubbles had more stiffer coating and less compression-expansion cycles then the lipid-based ones. Emulsification techniques were employed for the production of polymer-shelled microbbubles (Chlon et al., 2009).

2.3.4. Lipid-Coated Microbubbles

In biomedical imaging and drug delivery, lipid-coated microbubbles are the most commonly preferred ones (Sirsi and Borden, 2009). Because there are some advantages of phospholipid-coated microbubbles when they are compared with other types. First of all, they offer high flexibility and biocompatibility during perfusion. In addition to all these remarks, the exact goal is to use them in diagnostic and therapeutic applications

by ligand-receptor interaction between the microbubbles and the organ or tissue sites of interest (Borden et al., 2004; Unger et al., 2004).

The preparation of these lipid coated structures have been done with self-assembly techniques. After surfactants in the aqueous environment are transferred to the gas-liquid interface, the gas part diffuses out. On the interface, while the hydrophobic parts direct to the gaseous phase of the bubble, the hydrophilic head groups position towards the aqueous part. The production of a solid coating around the bubbles allows to obtain more stable microbubbles and prevent coagulation of them with other bubbles and biological materials (Klibanov, 2005).

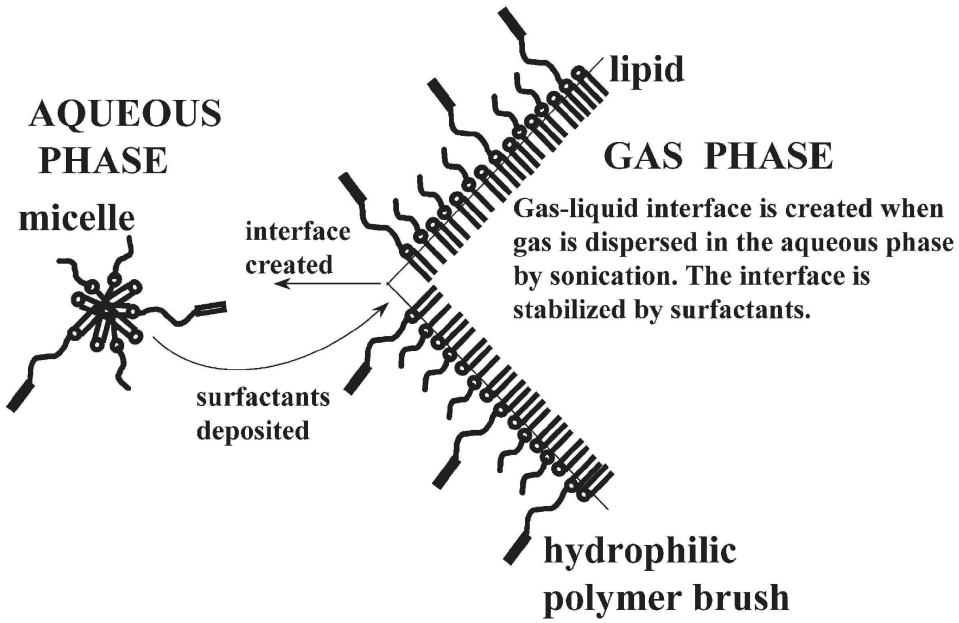

Figure 2.5. The structure of lipid-coated microbubble.
(Source: Klibanov, 2005)

The shell of the microbubble, is consisted of a main phospholipid constituent and an emulsifier containing a poly(ethylene glycol) (PEG) headgroup. This PEG tail on the phospholipid monolayer of the microbubble is used in the attachment of targeting ligands. Since the components of the bubble are entirely miscible, the shell is depicted as a homogeneous film. Although the components of the lipid monolayer shell is entirely miscible, it is in fact not. Borden and co-workers showed that the lipid shell is composed of polycrystalline areas around the emulsifier-rich and less organized parts in the expanded phase under fluorescent microscope (Ferrara et al., 2004).

The study of Klibanov and co-workers showed that the addition of hydrophilic polyethylene glycol (PEG) molecules to the microbubble monolayer shell served as a steric protection around them. Furhermore, the mixture of distearoyl phosphatidylcholine (PC) with a transition temperature of 55 ^{o}C and PEG stearate was able to maintain its structure for months in refrigerator (Klibanov, 2005).

The usage of phospholipid coating on the shells introduce several advantages. First of all, the shell is biocompatible and contains flexible properties to improve the perfusion of tissues. Moreover, it increases the stability of the coating shell under ultrasound. Also, some functional molecules can be easily joined together with the lipid layers. The aim is to find out the special ligand-receptor interactions in diagnostic and therapeutic applications (Klibanov, 2005).

CHAPTER 3

LANGMUIR MONOLAYERS AND THEIR PHASE BEHAVIOR

3.1. The History of Insoluble Monolayers

The discovery of oil-water interface phenomena began with Benjamin Franklin in 1774 (Moghaddam et al., 2011), and continued with Agnels Pockels, who found a new technique with a system containing a barrier and a trough parts in order to understand this fact. After that time, scientific achievements were carried out with Lord Rayleigh. He thought that there was a monolayer film structure between oil and water and he tried to find the thickness of these films (Chatterji and Rajdev, 2008; KSV LB Manual).

The Langmuir monolayers were proposed by Irving Langmuir in 1917 with the theoretical and experimental proofs of these insoluble monolayers at the air/water interfaces. Following these consequences, Katherine Blodgett found a new technique to transfer insoluble monolayers onto solid substrates in 1929. This technique is now known as the Langmuir-Blodgett (LB) technique and the layers coated on different substrates are called Langmuir films (Chatterji and Rajdev, 2008; Petty, 1996).

3.2. Fundamental Properties of Langmuir-Blodgett Technique

There are several techniques to get an organic thin film on a solid substrate. Some of them are self-assembly, electrodeposition, sputtering, thermal evaporation, molecular beam epitaxy, and also LB technique. Applications of thin organic films are seen especially in sensors, detectors and also in electronic circuits (Zasadzinski et al., 1994; KSV LB Manual).

LB technique is used to obtain an organic thin film on a solid substrate by spreading the mixtures on the surface of the subphase. Moreover, amphiphilic molecules, which are composed of hydrophobic (water insoluble) and hydrophilic

(water soluble) parts, are necessary for this technique. When these molecules are spread on the Langmuir trough, the hydrophilic parts point directly downward, and the other parts oriented in the reverse direction (Figure 3.1). While the hydrophobic part of them involves hydrocarbon or flurocarbon chains, the hydrophilic part is composed of a polar group like (-OH, -COOH, $-NH_3^+$, $-PO_4^-(CH_2)_2NH_3^+$ etc.) (KSV LB Manual) . The shematic representation of these amphiphilic molecules at the air/water interface are depicted in Figure 3.1.

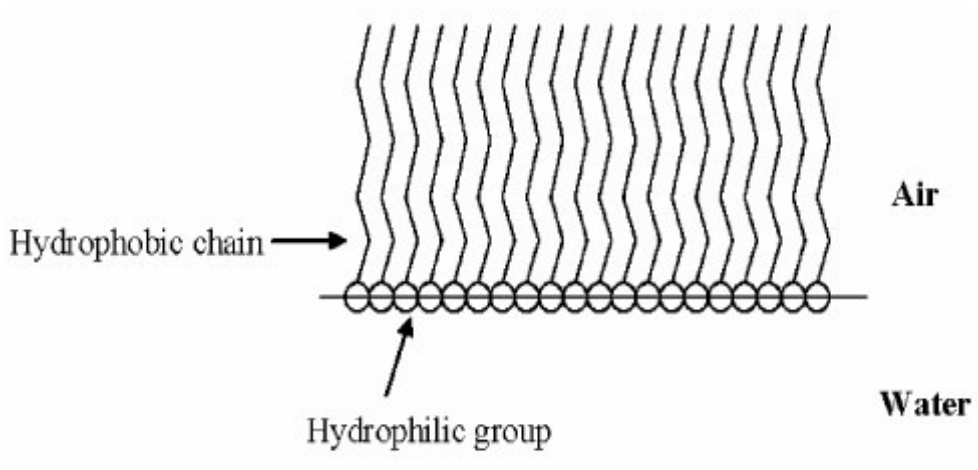

Figure 3.1. The representation of the amphilic molecules at the gas/liquid interface. (Source: Chatterji and Rajdev, 2008).

3.3. Monolayer Phase Behaviors at the Air/Water Interfaces

Some organic molecules are located at the air-liquid or liquid-liquid interface in order to reduce their free energy. Consequently, a surface film which is also known as a monolayer or a monomolecular layer, is obtained. The liquid-gas interface indicates a transition between two bulk phases. For each of the phases, there exists a surface layer with different properties (Petty, 1996).

The monolayers of amphiphilic molecules are insoluble at the air/water interface. These Langmuir films can be compressed with the symmetric barriers of the trough. This results an increase in the surface pressure values while the mean molecular

area is decreased. The surface pressure phenomena is the force per unit length exerted on the two-dimensional film (Meunier, 2000).

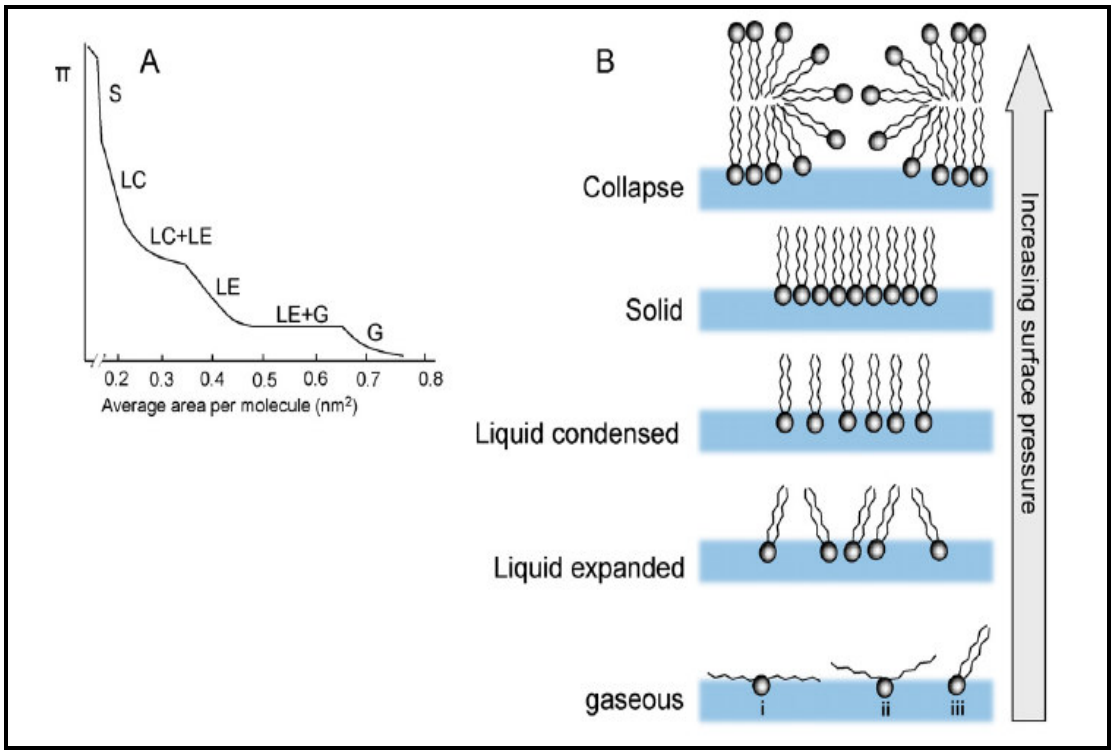

Figure 3.2. The schematic representation of (A) monolayer phases and (B) monolayer compression with the increasing surface pressure on the Langmuir isotherm. (Source: Moghaddam et al., 2011)

When the monolayer is compressed upon the barrier movement, phase transformations can be observed on the isotherms. The phase changes on the monolayer films at the air/water interface are shown in Figure 3.2. Initially, the gaseous (G) phase occurs. In this phase, the molecules are far enough apart from each other on the liquid subphase. There is little force between them. Upon further compression, the hydrocarbon chains of the amphiphilic molecules start to interact with each other. This phase is the liquid or expanded (E) monolayer phase. In liquid expanded (LE) state, the molecular orientations of the hydrocarbon chains of the molecules are random. When the surface area is reduced again, condensed (C) phases appear on the isotherm. In this phase, molecules are in regular orientation. The monolayer in the condensed phase is closely packed and the hydrocarbon chains of the amphiphilic molecules are oriented away from the water subphase. After compression at this phase results in a new

formation as the solid (S) phase. If the surface pressure increases with further compression, then the area of the film decreases and the film collapses on the subphase (Petty, 1996; Chatterji and Rajdev, 2008; Moghaddam et al., 2011).

3.4. Surface Pressure and Surface Tension

In dynamic molecular motion, many molecules tend to diffuse from the liquid phase to the surface per unit time. Once the molecule is reached to the surface, it is surrounded by fewer molecules. Therefore, the mean atomic separation and also the intermolecular forces increase when the molecules begin to diffuse from the surface . When the activation energy of a surface molecule is equal to the diffusing molecules, than an equilibrium state will be obtained. The force acting on this equilibrium line is called the surface tension and is denoted by γ (Petty, 1996).

This technique is based on the relationship between surface pressure and surface tension. In the formula given below (Table 3.1), Π is the abbreviation of the surface pressure and is measured with a pressure sensor attached to the trough, γ_0 is the surface tension before the spreading, and γ_m is the one after the mixture is spread on the LB trough (Moghaddam et al., 2011).

The surface tension of water is reduced when a monolayer at the air/water interface is decreased. The surface pressure of pure water is 72 mN/m, so this is the maximum value of this formula (Petty, 1996). The relation between surface pressure and surface tension is given by Equation (3.1).

$$\Pi = \gamma_0 - \gamma_m \tag{3.1}$$

There is a contradiction in terms of surface free energy between solids and liquids. Although this free energy can be calculated at the interfaces in solids, it is impossible to find out it in liquids. Futhermore, water which is a polar liquid, have strong intermolecular interactions and high surface tensions (Petty, 1996). If any factor interrupts these interactions, surface tension decreases. Thus, temperature, which is one of these factors increases, this will effect the whole system and surface tension decreases. The aim for using surfactants is to reduce the surface tension. At this point,

cleanliness is extremely important so as not to let any contamination into the system while searching the surface chemistry (Petty, 1996).

The surface pressure of the system is measured by a paper plate, which is also known as Wilhelmy plate. This plate is dipped into the aqueous subphase and indicates the differences in surface pressure values before and after the spreading processes on the subphases. There is vertical force acting on that plate. The related equations are given in Equation 3.2. In the equation, ρ_l is the density of the subphase, ρ_p is the density of the plate and g is the gravitational acceleration acting on that plate. Equation (3.2) involves several parameters, which are denoted clearly on the Figure 3.3.

$$\text{Force} = (\rho_p lwt)\, g - (\rho_l dwt)\, g + 2\,(w+t)\,(ST)\cos\theta \qquad (3.2)$$

ρ_l = density of the subphase.
ρ_p = density of the plate.
g = gravitational acceleration acting on that plate.
l = length of the plate.
w = width of the plate.
t = thickness of the plate.
d = depth of the subphase solution.

The gravity and surface tension forces are acting downwards into the subphase, and also the buoyancy force is acting in the upward direction to the water. Since the plate is at constant position, uptrust term is eliminated in equation 3.3 (KSV LB Manual).

$$\text{Force} = \text{Weight} - \text{Uptrust} + \text{Surface Tension} \qquad (3.3)$$

3.5. LB Film Deposition

LB technique is employed for the construction of mono or multilayer films. By transferring monolayers onto many substrates, the LB technique is unique in thin film deposition. In this technique, amphiphilic molecules on the air-water interface are transferred to an appropriate substrate. The first organized, uniform monolayers were

obtained by this technique. Today, this technique is stil the most extensively studied one (Petty, 1996).

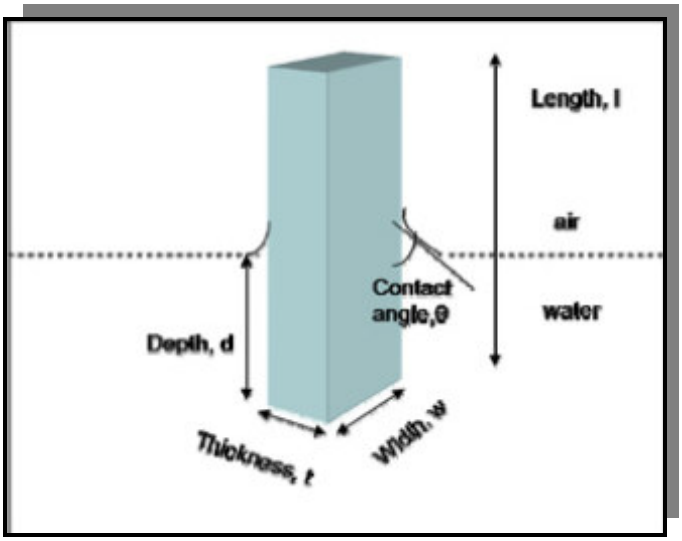

Figure 3.3. The representation of the dimensions of the Wilhelmy (paper) plate.
(Source: Chatterji and Rajdev, 2008)

LB film deposition can be done onto both hydrophilic or hyrophobic substrates. The monolayer on the subphase is expected to transfer to the substrate without altering the molecular orientation of the film (Zasadzinski et al., 1994; Petty, 1996). The thickness of the surface layer plays an important role in molecular forces. Short-range forces occur when the molecules are electrically neutral. On the other hand, charged molecules allow to extend the transition region to larger distances (Petty, 1996).

There are three kinds of deposition techniques in LB dipping system. The deposition type showed in Figure 3.4 is the Y-type one. In this type, the head groups are attached with the head groups, and the hydrocarbon tails with the tails. In other words, molecular interaction occurs between the tail of one amphiphile with the tail of another one; also, the head parts with the same idea. As shown in Figure 3.4 (2), upstroke movement is done to the substrate (Chatterji and Rajdev, 2008).

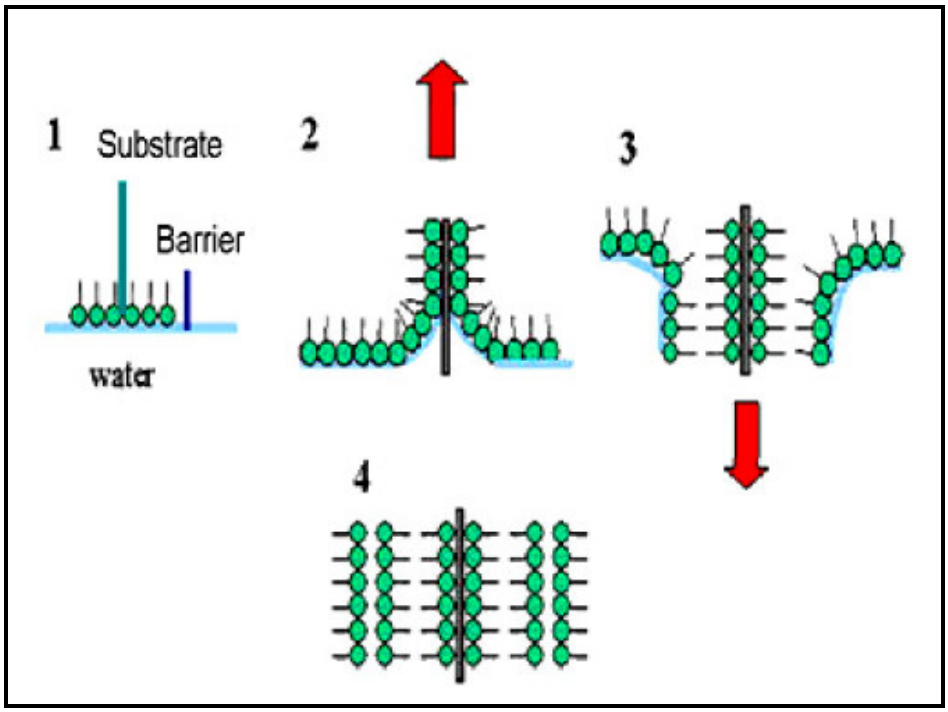

Figure 3.4. The schematic representation of monolayer deposition.
(Source: Chatterji and Rajdev, 2008)

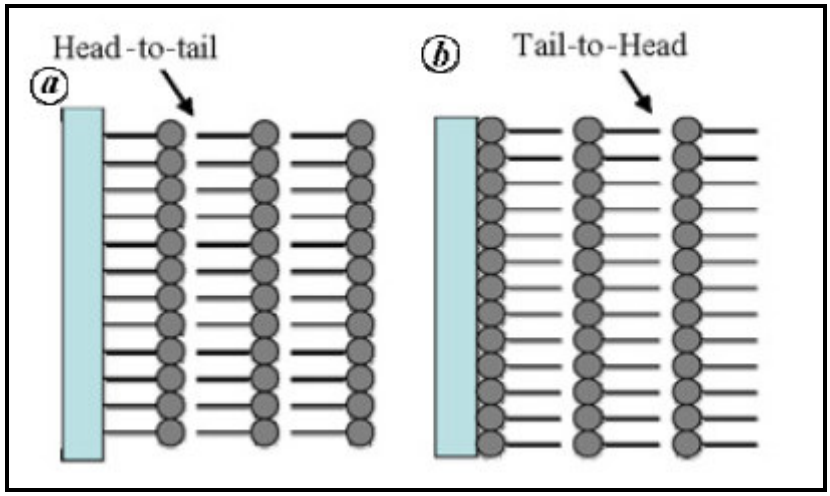

Figure 3.5. Different deposition techniques in LB dipping process; (a) X-type deposition and (b) Z-type deposition. (Source: Chatterji and Rajdev, 2008)

The other type of depositions are depicted in Figure 3.5. If a hydrophobic substrate is used, then head-to-tail deposition, which is known as the X-type deposition Figure 3.5 (a), is obtained with the upstroke movement of the substrate. The last type is the Z-type deposition Figure 3.5 (b). Z-type films are obtained with hydrophilic

substrates. The head groups are rejected by the hydrocarbon tail groups and forms tail-to-head interactions. The deposited film is formed by the upstroke movement of the substrate. The most stable deposited film is the X-type one among others (Chatterji and Rajdev, 2008).

Several techniques including X-ray scattering, phase behavior, fluorescence microscopy and Brewster angle microscopy allow to obtain information from the Langmuir monolayers at the air/water interface. Additionally, if the deposition is done onto substrates, then these data can be compared with other techniques like the experiments done with X-ray diffraction, electron diffraction and scanning force microscopy (Zasadzinski et al., 1994).

CHAPTER 4

EXPERIMENTAL

The experimental part of this thesis study involved monolayer formation on the air/water or on physiological buffer subphases for different ionic strength conditons. LB technique was used for the monolayer formation and the characterization of these monomolecular films were done by Brewster angle microscopy (BAM) at the liquid-gas interfaces.

4.1. Materials

DSPC (1,2-Distearoyl-sn-glycero-3-phosphocholine) was the main phospholipid component and polyoxyethyleneglycol stearate (PEG 40 S) was the emulsifier used in the experiments. DSPC with purity ≥99 % and non-ionic emulsifier (PEG 40 S) were both purchased from Sigma. Since these chemical materials were solid in room temperature (25°C), chloroform ($CHCl_3$) which was purchased form Merck with the purity of 99-99.4 % was used as a solvent to prepare spreading solutions with 1 mg/ml (1:1) concentration for the monolayer formation. The chemical formulas of these amphiphilic molecules are illustrated in Figure 4.1.

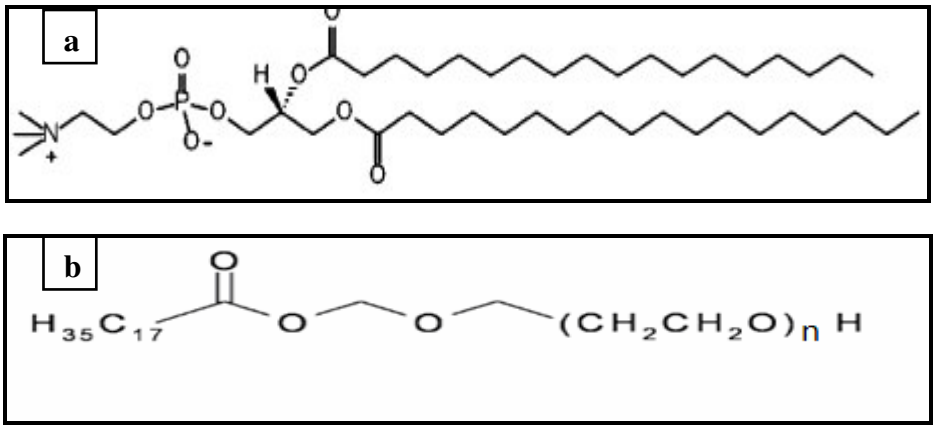

Figure 4.1. The chemical formulas of the materials (a) DSPC, (b) PEG 40 S.

In addition to the pure components, their mixtures with different ratios were prepared to find out the effect of surfactants and the mixing ratio. Mixtures of DSPC-PEG 40 S were prepared at the molar ratios of 9:1 and 8:2. The effect of molecular interactions between the emulsifier and the phospholipid molecule were investigated for these mixtures in different subphases.

The buffer effect was investigated with sodium phosphate ($NaH_2PO_4.H_2O$ and Na_2HPO_4) buffer saline. The main used salt was NaCl; only in one buffer solution, NaCl and $MgCl_2$ addition was done to see the differences. Ultra pure water and phosphate buffer solutions at different ionic strengths were used as the subphases . The ultra pure water (18.2 MΩ.cm) used in the KSV LB minimicro system was obtained form Millipore-Milli Q Gradient system.

All mixtures were stored in a glass container at -22 °C. These solutions were prepared in a two-week period of time so as to maintain the concentration of them. Before spreading the solution on the subphase, it was sonicated for 10 minutes in order to homogenize the solution. All the experiments were carried out at ambient temperatures.

4.2. Sample Preparation for The Experiments

4.2.1. The Preparation of Buffer Solutions

The effect of ionic strength (I.S.) was investigated in a through way with the buffer solutions (Table 4.2) used as the subphase at pH of 7.2. The subphase of the monolayers contained different values of salt additions. The buffer ionic strength of the subphase solutions was kept constant (40 mM) in buffer 1, 2 and 3 solutions. Total ionic strength was varied via addition of different amounts of NaCl as shown in Table 4.1. In addition to this salt, in buffer 4, $MgCl_2$ was also been added to the buffer 3 composition so that different salt effects on the monolayer formation were investigated.

4.3. Langmuir-Blodgett (LB) Technique

Langmuir-Blodgett trough (KSV minitrough) with movable barriers was used to

measure the surface pressure-mean molecular area of the monolayers. The trough was enclosed in a box to minimize the possible contamination onto the air-monolayer-water interface and the disturbance of the monolayer by air currents (Figure 4.2).

Prior to the each experiment, the Langmuir trough and its barriers were brushed with ethanol and rinsed with ultra pure water. After this cleaning process, the subphase was added to the trough and the paper plate was hanged on its place. As a surface balance on the subphase, a paper plate, Wilhelmy plate, was used.

Table 4.1. The ionic strength of the buffer solutions used as the subphases.

	Buffer Ionic strength (I.S.) (mM)	**NaCl Ionic strength (I.S.) (mM)**	**$MgCl_2$ Ionic strength (I.S.) (mM)**	**Total Ionic strength (I.S.) (mM)**
BUFFER 1	**40**	**0**	**0**	**40**
BUFFER 2	**40**	**80**	**0**	**120**
BUFFER 3	**40**	**120**	**0**	**160**
BUFFER 4	**40**	**120**	**20**	**180**

Cleanness of the subphase was confirmed via surface pressure measurement. If the surface pressure measured in the absence of monolayer exceeds 0.3 mN/m, it meant that the upper part of the subphase involved dust or some other molecules from other experiments. In our measurements, surface pressure readings changed between 0.09-0.3 mN/m before all the monolayer formation measurements.

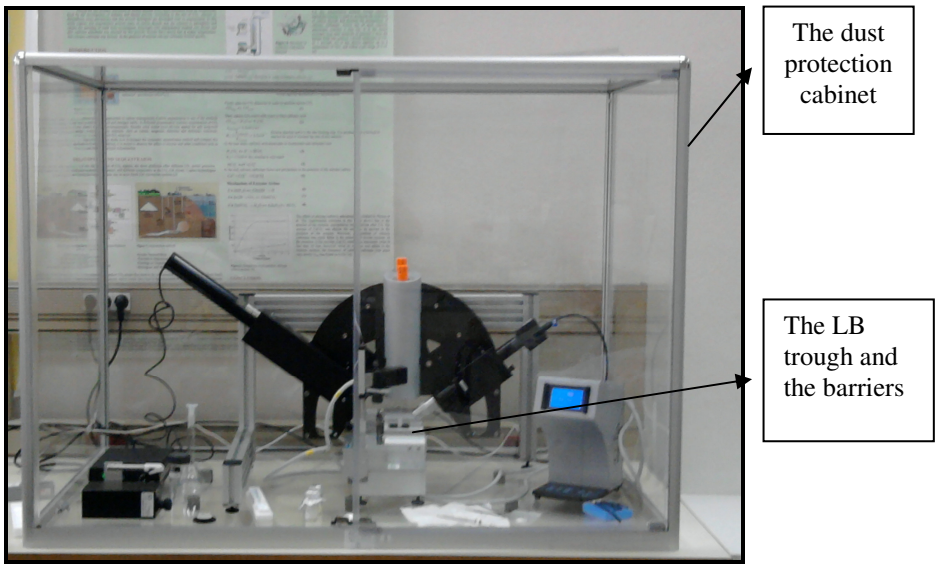

Figure 4.2. The dust free cabinet for the Langmuir-Blodgett system.

Spreading solutions of DSPC-PEG 40 S at predetermined molar ratios (9:1 and 8:2) with the concentration of less than 1.0 mg/ml in chloroform were prepared and spread on the subphase via a Hamilton microsyringe. After spreading the molecules onto the subphase, it was allowed 20 minutes for the evaporation of chloroform. The surface pressure-area (π-A) isotherms were obtained via symmetric compression of the monolayers by two barriers. A compression speed of 5 mm/min was used in all experiments.

4.4. Characterization Techniques

4.4.1. Brewster Angle Microscopy (BAM)

4.4.1.1. The Physics Behind The BAM

Brewster angle microscopy technique, which is employed for the visualization of thin films, is a non-invasive technique. Generally, this technique is utilized to characterize the monolayers like Langmuir films at the air/water interface (KSV Optrel BAM 300).

The principle behind this technique is based upon reflectivity of light at a specific angle, known as the Brewster angle. Brewster angle is the angle of incidence of the polarized light. The light is reflected and partially polarized after striking a surface as is shown in Figure 4.3. The polarization and the angle of incidence is directly related with the reflectivity of light (Meunier, 2000; Hecht, 2002).

The Brewster angle is found by the known refractive indexes of several substrates such as the refractive index of air/water interface is 1.333 and air/glass is 1.515. This special angle for a beam of light traveling through air can be calculated by the Snell's Law as is shown in equation 4.1 (Hecht, 2002).

$$n = \sin(\theta_i) / \sin(\theta_r) = \sin(\theta_i) / \sin(\theta_{90-i}) = \tan(\theta_i) \quad (4.1)$$

In this equation, n is the refractive index of the medium from which the light is reflected. The angle of incidence and refraction are denoted by θ_i and θ_r, respectively (KSV Optrel BAM Manual).

Before spreading the solutions on the subphase, there is not a reflection from the water surface. As a result of the visualization of that surface with vertically polarized light at the specific angle, Brewster angle, a black background is obtained. There is an example of this reference background (Figure 4.4) obtained in our experiments.

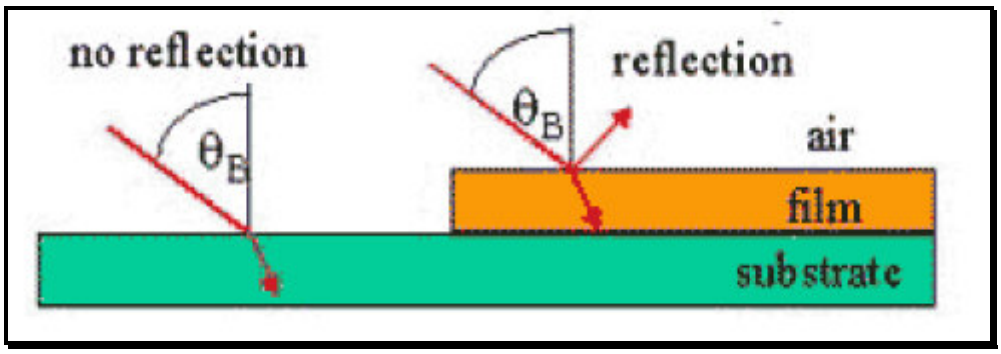

Figure 4.3. Schematic representation of the reflection light from a dielectric or insulating media and also how the polarization of light is changed. (Source: Optrel BAM Manual)

After spreading a solution on the subphase, or deposited on a substrate, the reflectivity changes. Since the monolayer spread on the interface is in nano scale, it has a tiny effect on the monolayer visulization (KSV Optrel BAM 300). The alteration of this background image after spreading the solutions saved and depicted in Chapter 5.

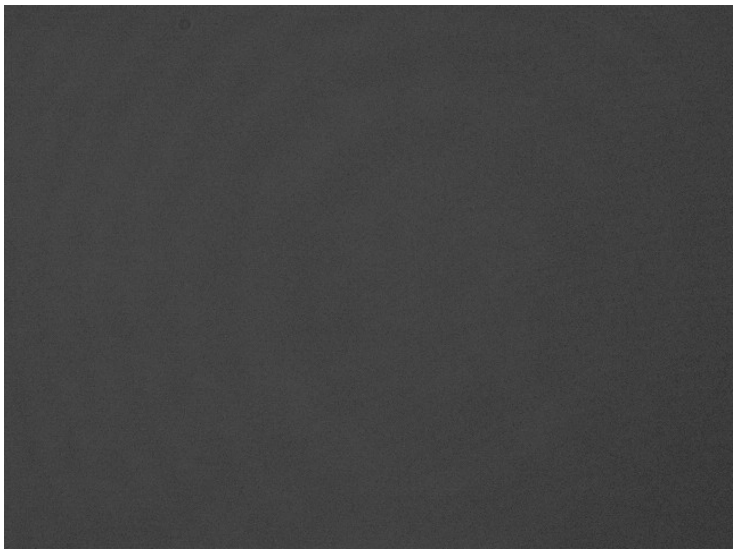

Figure 4.4. The reference background image obtained before the spreading process.

4.4.1.2. BAM Measurements

In our system, the Brewster angle microscope (KSV Optrel BAM 300, standard HeNe laser) was placed over the KSV Langmuir-Blodgett Minitrough system (Figure 4.5). The magnification of the objective was 10x. This laser induced system was employed for the characterization of the monolayer coating at the air/water or buffer interfaces. For the BAM measurements, the power of the laser was turned on an hour at the beginning of the measurements. The Langmuir trough and the barriers were cleaned as described in part 4.3.

The black glass plate used for BAM measurements was cleaned with ethanol and ultra pure water. The mechanical shutter of the laser was kept closed at first so as to avoid exposure to the beam by direct looking into it or its reflected parts. The trough, barriers and the black glass plate were placed under the BAM system. After filling the trough with pure water or buffer solutions, cleanliness was controlled as described in part 4.3. The subphase level in all experiments was kept constant (175 ml).

After the adjustments of the Langmuir trough, the mechanical shutter was opened after lowering the goniometer at the edge of the trough.

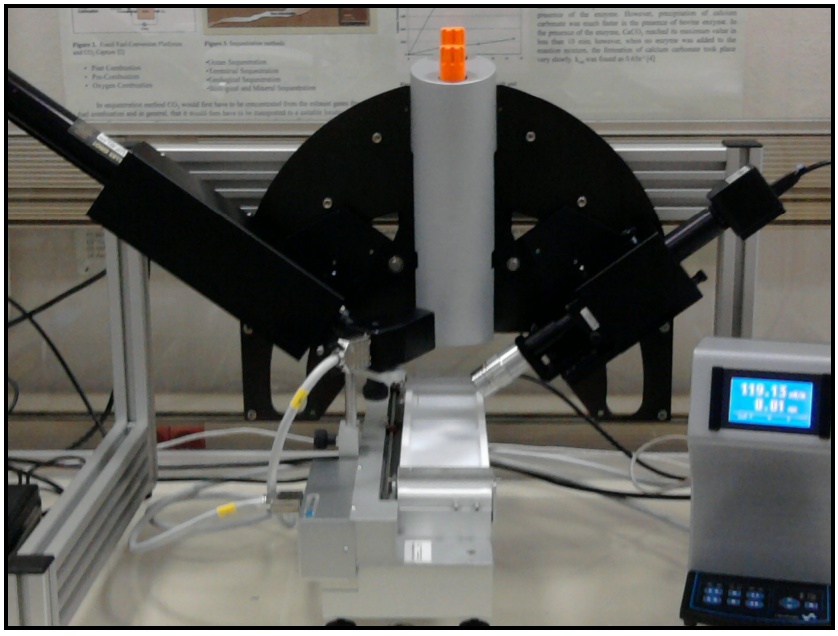

Figure 4.5. The Brewster angle microscope and the Langmuir-Blodgett system based in Chemical Engineering Department, IYTE.

The orientation of the black glass plate, shown in Figure 4.6, is very important because the wedge-shaped part must be in the same direction with the laser beam. The laser beam collides at the mid-point of the wedge-shaped part (KSV Optrel BAM 300 Manual).

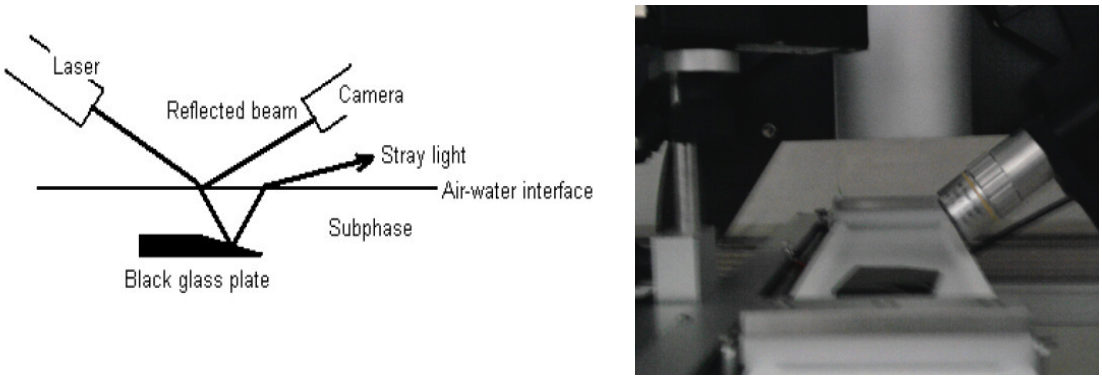

(a) (b)

Figure 4.6. The position adjustment of the black glass plate, (a) the direction of the laser beam (Source: KSV Optrel BAM 300 Manual), (b) finding the optimum place for the black glass.

After the adjustments of the Langmuir trough and the camera, the BAM 300 software was started. The height and the angle of the goniometer was adjusted simultaneously to set the system at Brewster Angle, which was known as 53^{o} at air/water interface. During the adjustment, it was ensured that laser beam hit the wedged part of the black glass plate.

The settings of the camera were set to the same values through all the BAM measurements. 1/50 seconds were chosen for the shutter timing as exposure and the gain value was 657 dB. Also, brightness and auto reference parameters were adjusted to zero in the analysis. The camera, LB trough, barriers and the black glass plate adjustments were the same in all BAM experiments. The difference on the monolayer features came out from the spreading solutions on different subphases. Thus, the molecular interactions between the solutions and the subphase resulted in different conformations such as bright or dark regions on the images.

CHAPTER 5

RESULTS AND DISCUSSION

Surface pressure-area isotherms are the beneficial ways for the characterization of the phase behaviors of Langmuir monolayers. There are some separate single-phase regions in the isotherms indicating the differences between monolayer states. These amphiphilic monolayers are described as gaseous (G) phase after the evaporation of the spreading solution, liquid expanded (LE) phase with disordered monolayer structure on the subphase, liquid condensed (LC) and solid condensed phase with an ordered monolayer structure. Passing from one single-phase to another like the transition between LE and LC, and also between G and LE phases indicate the coexistence of these two different phases. The coexistence of LE and LC phases result in plateau regions on the isotherms as a first-order phase transition (Ma and Allen, 2006; Degen et al., 2005).

In this study, the monolayer structure of pure molecules and mixed monolayers were studied by using surface pressure-area isotherms and Brewster angle microscopy images on different subphase conditions. The related isothermal graphs are seen in Figure 5.1.

5.1. The Subphase Effect on Pure Molecules

5.1.1. LB Isotherms

The isotherm in Figure 5.1(a) shows the surface pressure-area isotherm of pure DSPC at the air/water interface. Since there is not a plateau region between LE and LC phases, then there is not a phase transition between them (Degen et al., 2005).

The isotherm of DSPC in Figure 5.1(a) starts to increase immediately at a molecular area of approximately 55 A^2 per molecule. When the surface area is decreased, the slope of the isotherm increases and the monolayer becomes more condensed.

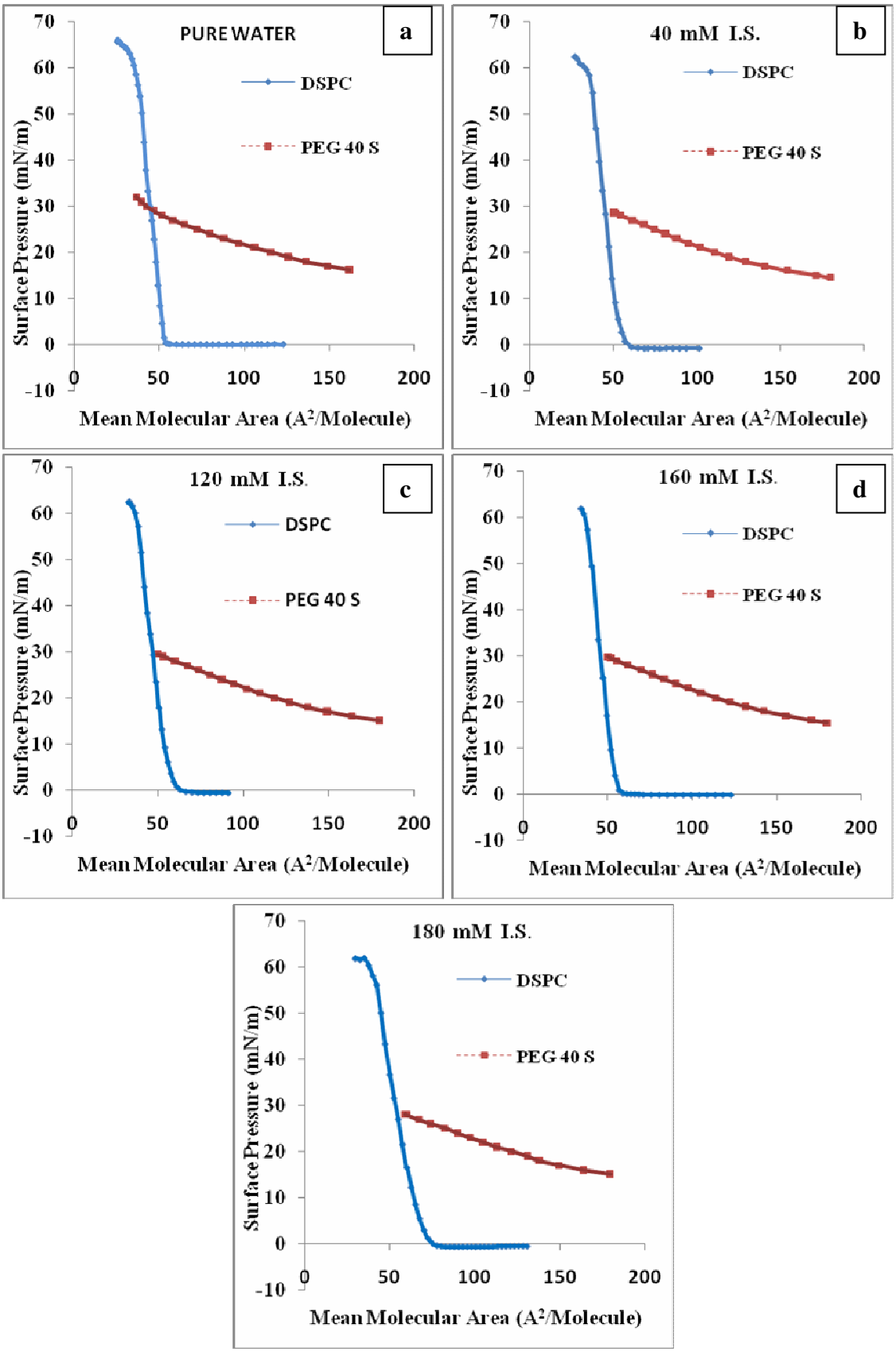

Figure 5.1. The isotherms of pure molecules on (a) pure water and phosphate buffer solutions at b) 40 mM, c) 120 mM, d) 160 mM, e) 180 mM I.S.

The slope of the DSPC isotherm indicates a compact, rigid monolayer formation on the water subphase (Arnold et al., 2005). The surface pressure-area isotherm of DSPC on the water subphase was already investigated by other researchers (Kubo et al., 2001; DeWolf et al., 1999).

In the isotherm, 0-1 mN/m surface pressure interval indicates the gaseous phase. While the surface pressure increases, G phase disappears and a short LE phase comes out between 1-4 mN/m. After this phase, LC phase appears between 4-60 mN/m. The phospholipid monolayer collapses upon further compression, and this occurs above 60 mN/m.

The isotherm of the emulsifier in pure water and PBS subphases are also shown in Figure 5.1(a-e). The pure PEG 40 S isotherm at the air/water interface is consistent with the literature (Borden et al., 2004). The isothermal graphs of PEG 40 S begins at high surface pressures. This is because of the repulsive interactions acting on the hydrophilic PEG chains as already explained in the study of Borden and his group (Borden et al., 2004). During the compression process of the system, PEG 40 S exists in the condensed phase.

Although these two amphiphilic molecules have the same hyrophobic chain length, the collapse point is less distinct for PEG 40 S when it is compared with DSPC isothermal graph.

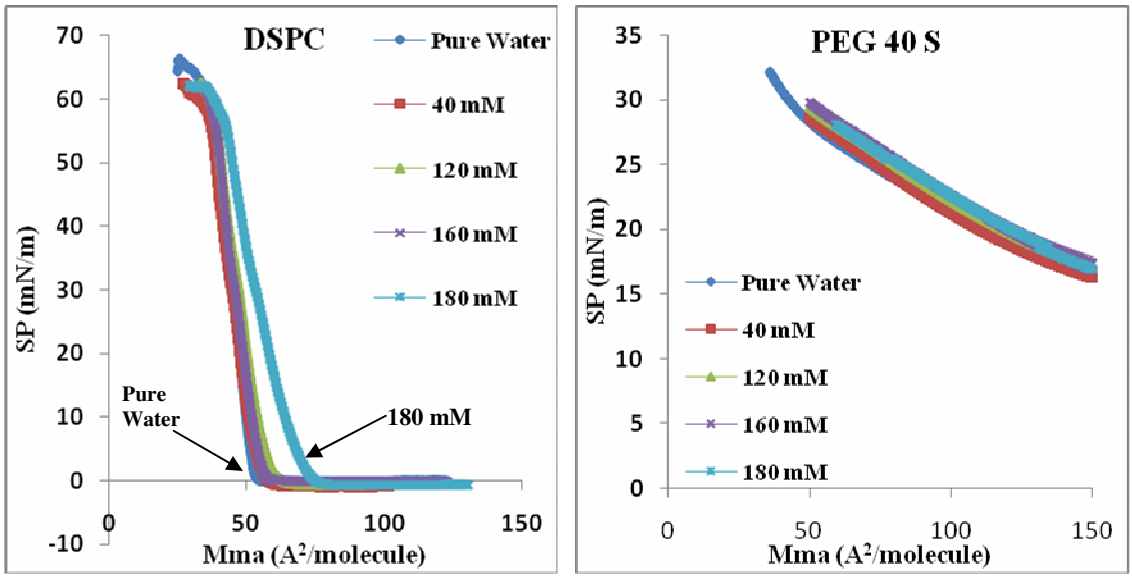

Figure 5.2. The surface pressure-area isotherm of (a) DSPC and (b) PEG 40 S on subphase of pure water and phosphate buffer solutions at different salt I.S.

The isotherm of DSPC indicates different phase regions as it is observed in pure water condition in Figure 5.1(a). The effect of ionic strength was investigated by using different phosphate buffer solutions. Additionally, the effect of different salts, NaCl and $MgCl_2$, were examined with surface pressure-area isotherms and Brewster angle miroscopy images.

When the DSPC isotherm on pure water is compared with the isotherm obtained on 180 mM ionic strength condition, it can be seen that the buffer solution containing NaCl and $MgCl_2$ salts is shifted to a higher mean molecular area (Figure 5.2(a)). The LE phase region and the collapse pressure values are also shifted. There is not a plateau region in both of the isotherms so there is not phase transtion between LE and LC phases. Therefore, it can be said that the pure water subphase forms a more compact monolayer structure since it is shifted to a lower mean molecular area value.

In Figure 5.2(b), the surface pressure-area isotherms of the emulsifier under the buffer conditons are shown. There is not a noticeable difference between these isothermal graphs. Like on the pure water subphase, the reason of high surface pressure is due to the repulsive forces acting on the hydrophilic PEG chains (Borden et al. 2004).

5.1.1.2. BAM Images

A series of BAM images were taken during the compression of DSPC and PEG 40 S monolayers at the air/water interface. The BAM images of DSPC are represented in Figure 5.3.

According to the images obtained at different surface pressures, DSPC formed condensed and homogeneous monolayer structures on the water surface. Therefore, as observed in other studies as well, BAM images of DSPC do not show any phospholipid domains (Kubo et al., 2001; Hollinshead et al., 2009; Arnold et al., 2005; DeWolf et al., 1999; Barlow et al., 2007). The squeeze out plateau can be seen in Figure 5.3 (1) on DSPC monolayer at the air/water interface. Before this conformation, there is not a heterogeneous structure observed on the monolayer. The smoothness of the surface dissappears with the collapse pressure.

The same analysis done with another double-chain phosphocholine with 16 hydrocarbon tails, DPPC, showed the similar results at the air/water interface (Lawrie et al., 2000; Kubo et al., 2001; Hollinshead et al., 2009).

The homogeneous structure continues until the surface pressure of DSPC increases and reaches the collapse pressure. This condensed monolayer dissappears at 63.02 mN/m surface pressure. As a result of this analysis, if there is no additional molecule in the spreading mixture, the pure double chain phosphatidylcholine lipids do not exhibit phospholipid domains at the air/water interface. When the BAM data of DSPC on pure water is compared with its Langmuir isotherm in Figure 5.1(a), then it can be seen that the isotherm begins to increase with a steep slope after the gaseous phase. The increase of the surface pressure of this molecule was explained in a study as the compactness and rigidity of the DSPC monolayers (Arnold et al., 2005). Thus, the condensed monolayer film images of DSPC as shown in Figure 5.3 are consistent with the isothermal data.

The BAM images of PEG 40 S on the water subphase (Figure 5.4) display patterns of heterogenous parts. There is not a significant difference between these images. Upon compression, bright patches are seen. This is related with the condensed phases of the emulsifier on the water subphase.

Figure 5.5 shows the BAM images of DSPC on the subphases containing different salt ionic strengths. The images were taken at different surface pressures. When it is compared with the water subphase (Figure 5.3), the buffer conditions shows some differences. When the surface pressure is increased, the homogeneous monolayers are observed around 25 mN/m, but when the compression continues, then the condensity increases and bright images come out.

As a result of the differences in surface density or monolayer thickness, BAM images have different conformations. Bright images are observed in condensed phases and dark ones are belong to expanded phases. When compared with the air/water interface (Figure 5.3), observations with pure molecules in buffer solutions (Figure 5.5) display more condensed images.

When the ionic strength is increased, there are no inhomogenities on the subphase at low surface pressures on 120 mM buffer solution (Figure 5.5). However, when the surface pressure is increased, there becomes heterogeneous structures appeared on the monolayer films. Phospholipid pathches are seen throughout the compression. The dark background of the surfaces is continuously observed until it

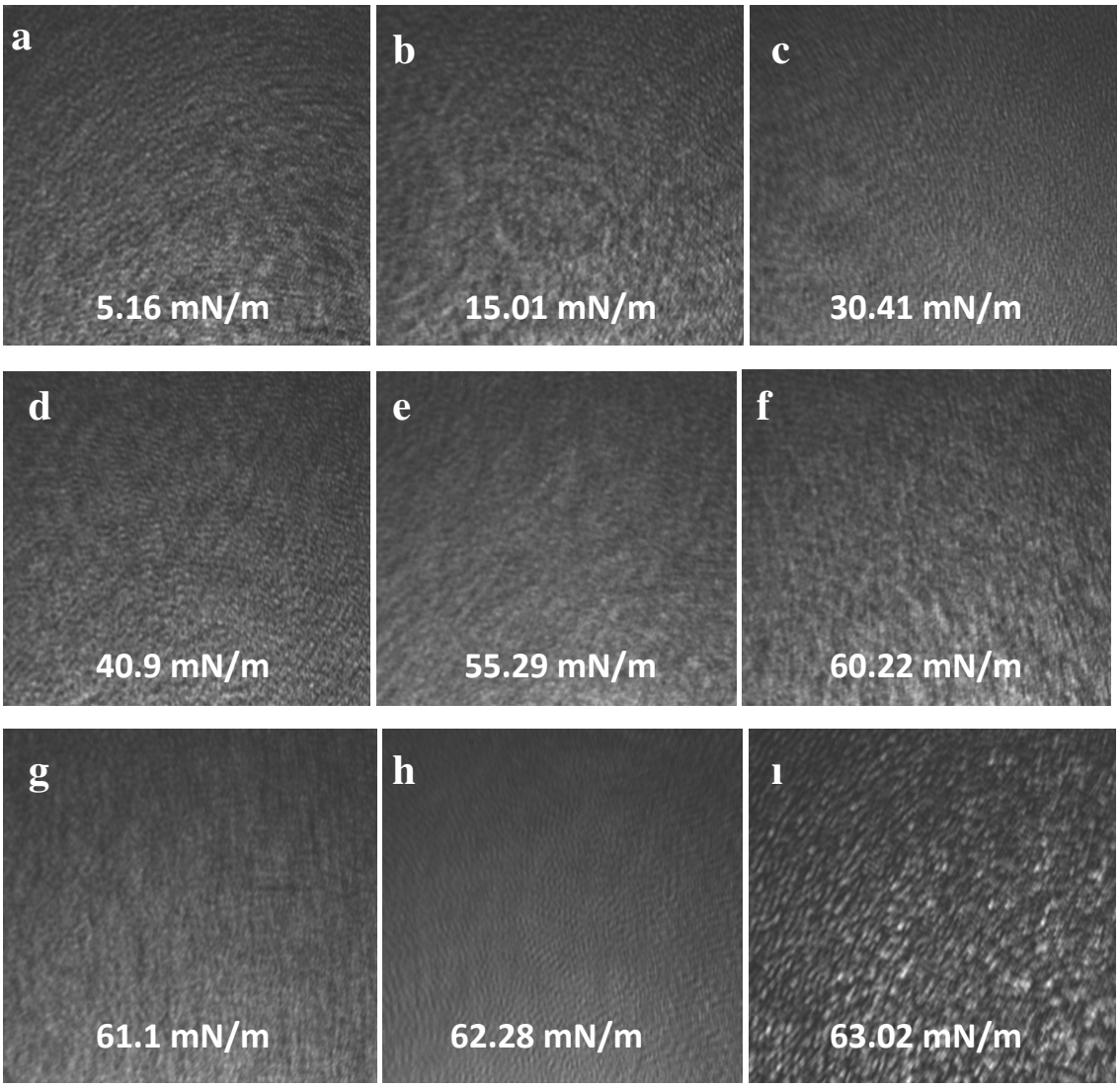

Figure 5.3. The BAM images of DSPC on pure water subphase at ambient temperature with surface pressure values. The image scale is 400 x 300 µm.

reaches the colllapse pressure of 64 mN/m. Initially, the monolayer was in the G-LE phase around 5 mN/m surface pressure. The monolayer indicates relatively brighter structure when it is compared with the other solutions at that surface pressure. When the compression proceeded, some dark areas are appeared on the subphase indicating the disordered regions of the monolayer.

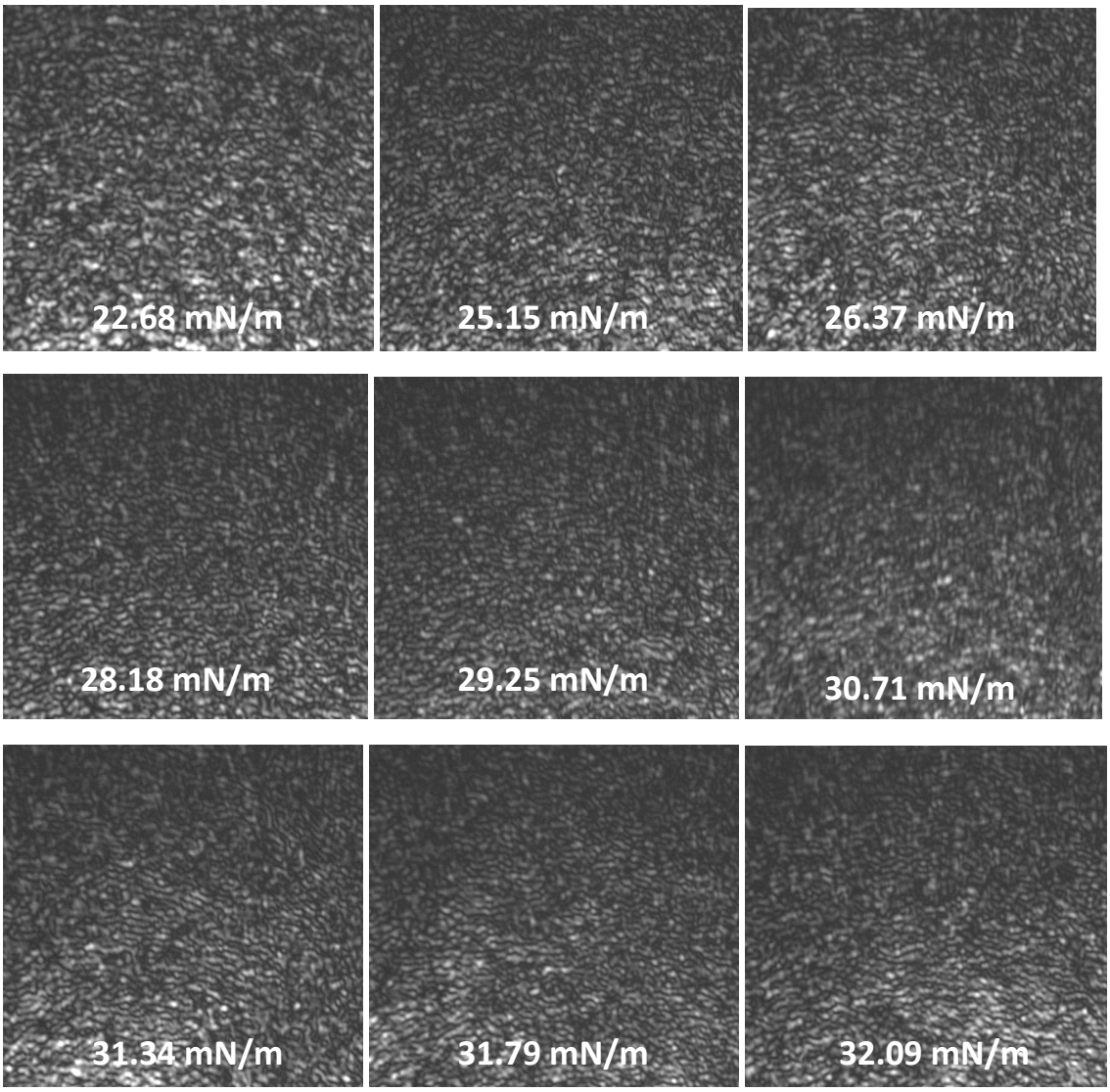

Figure 5.4. The BAM images of PEG 40 S on pure water subphase at ambient temperature with surface pressure values. The image scale is 400 x 300 µm.

According to Heckl et al., the change of the ionic strength affects the area of the choline head group of the molecules. They used fluorescence microscope to investigate the molecular interactions at the air/water interface and found the spiral domains on the films at high ionic strength conditions. They considered that the head groups of the molecules had electrostatically tilted and formed domain aggregation (Heckl et al., 1986; Basnet, 2010). In addition to this study, according to the Gouy-Chapmann theory, the high ionic strength condition also affects the molecular interactions (Helm et al., 1987).

In our study, BAM was employed to investigate the domain formation on the monolayer and we observed the spiral domains on the surface of the subphases. It seems

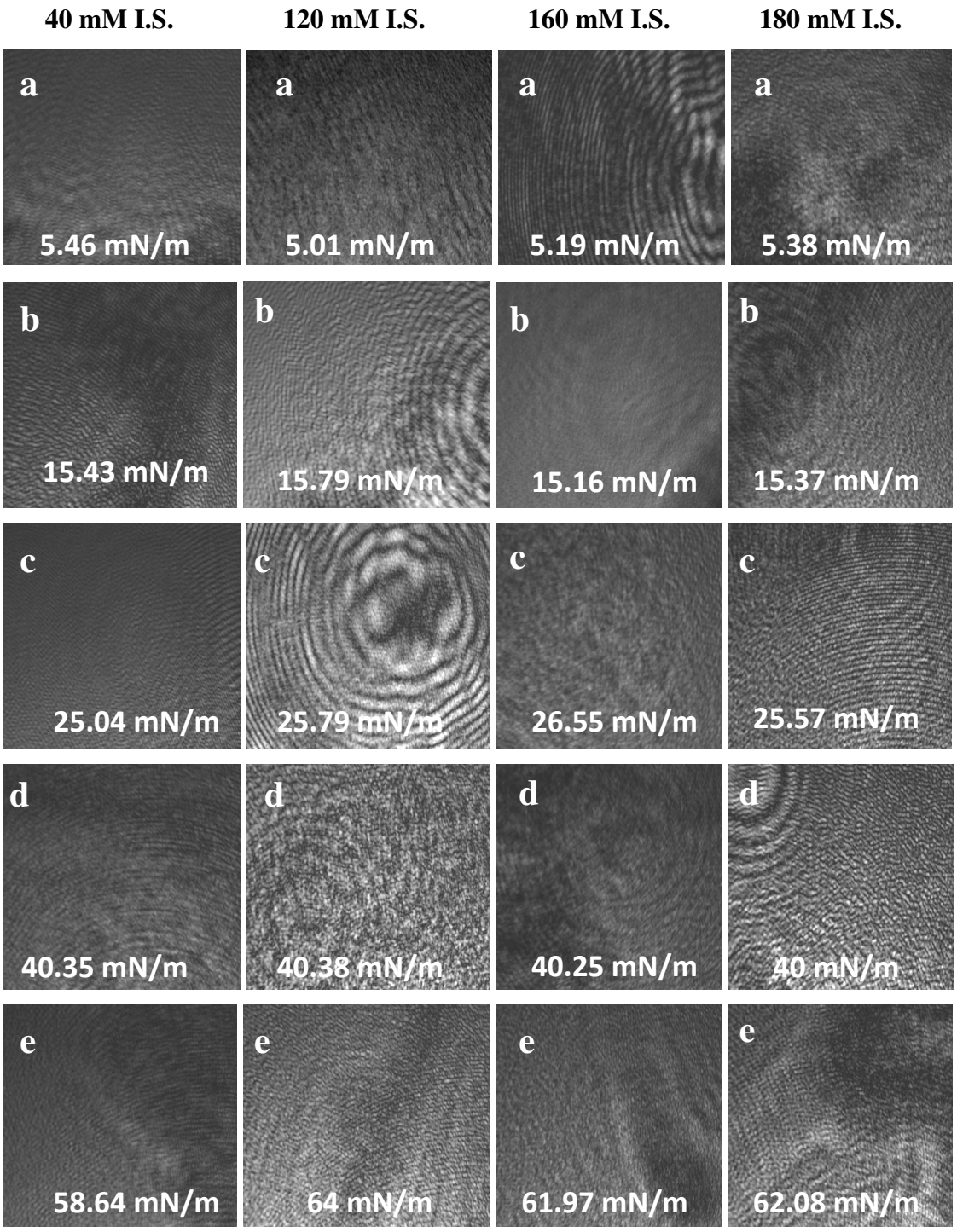

Figure 5.5. The BAM images of DSPC on different buffer conditions at ambient temperature with surface pressure values. The image scale is 400 x 300 µm.

that the 40 mM ionic strength does not affect the head group of the DSPC molecule very much. Besides, when the ionic strength is increased, molecular interactions are altered and forms spiral structures.

5.2. The Subphase Effect on Mixed Monolayers

5.2.1. LB Isotherms

Several studies were done for the investigations of the mixed monolayers of DSPC and PEG 40 S. The mixtures of DSPC-PEG 40 S were prepared at the molar ratios of 9:1 and 8:2. The effect of molecular interactions between the emulsifier and the phospholipid molecule were investigated for these mixtures in different subphases.

Figure 5.6 (a) shows the surface pressure-area isotherms of the 8:2 and 9:1 mixed monolayers at the air/water interface. There is a positive trend between pure molecules and mixtures. The 8:2 and 9:1 mixtures display more condensed monolayers since they are shifted to a less mean molecular area value.

The gaseous phase is not observed in the 8:2 and 9:1 DSPC-PEG 40 S isotherms. This indicates the existence of repulsive forces between hydrophilic PEG molecules. These interactions results in high surface pressure in the mixture like being observed with the pure PEG molecules.

Upon compression, there is a gradual increase in surface pressure for the 8:2 mixed monolayer. There is a plateau regime in the isotherm indicating that there is a transition between LE and LC phases. The expanded phase of this isotherm starts approximately at 80 A^2 per molecule area and upon further compression, this phase continues until it reaches the plateau region that shows the first-order thermodynamic transition.

The 9:1 DSPC-PEG 40 S mixture also involves a distinct plateau region like the 8:2 mixed one as seen in Figure 5.7 (b). Upon compression, there is a sudden increase observed between 40-50 A^2 per molecule area. From this area to the collapse pressure point, condensed phases are dominant. According to the study of Borden and co-workers, 9:1 DSPC-PEG 40 S isotherm at the air/water interface also shows a plateau region on the isotherm with the comparison of the saturated phosphocholine lipids, like the DSPC molecule (Borden et al., 2004).

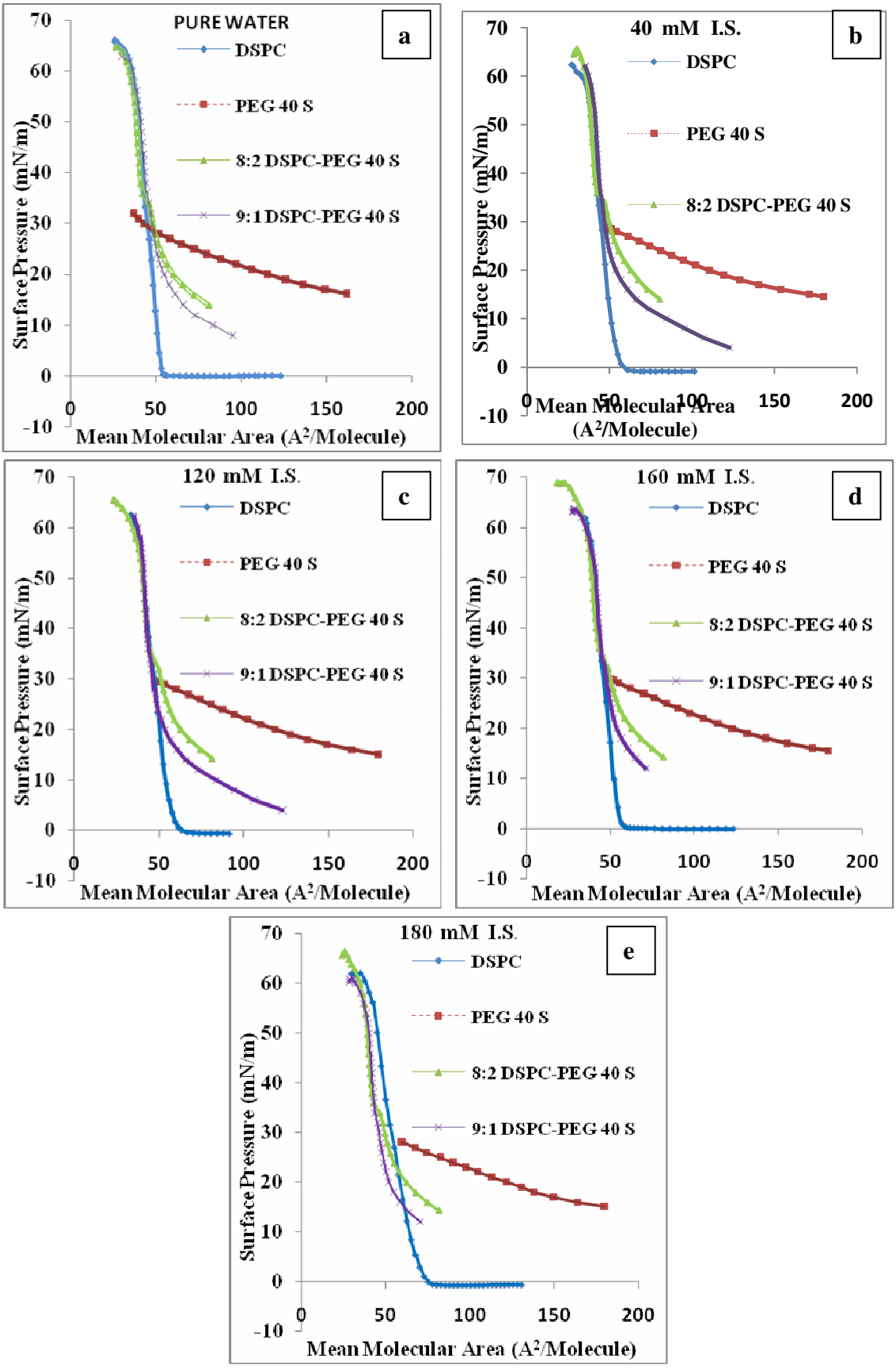

Figure 5.6. The isotherms of pure molecules on (a) pure water and phosphate buffer solutions at b) 40 mM, c) 120 mM, d) 160 mM, e) 180 mM I.S.

The Langmuir isotherms of the 8:2 and 9:1 DSPC-PEG 40 S under the buffer effects are shown in Figure 5.6 (b-e). For the 8:2 mixed monolayers, distinct regions are noticable, except the gaseous phase in both of the figures as it was observed with the pure water subphase.

The reason of the high surface pressure is due to the repulsive attractions between PEG molecules. The isotherm begins with the expanded phase and forms a plateau region like the one obtained with the water subphase. Again the plateau region is identical for the 8:2 mixture showing the phase transition between liquid expanded (LE) and liquid condensed (LC) phases.

In order to analyze the buffer effect on the same composition mixtures containing two different molar ratios are given separately in Figure 5.7. Generally, the characteristic plateau region for the 8:2 DSPC-PEG 40 S mixed monolayer disappears at about 40 A^2 /molecular area upon compression. There is a slight difference between 40 mM and 120 mM total ionic strength for this mixture (Figure 5.6(b) and (c)). Further compression results in higher surface pressure and the monolayer film collapses at around 65 mN/m surface pressure.

The difference in collapse pressure can be the result of the alteration of the molecular interactions in the buffer media because their molecular compositions are the same (Lucero et al., 2008). Therefore, since the molar ratios of the mixtures are different from each other (8:2 and 9:1), then their collpase pressure values allow to obtain the information about the cohesive forces between the hydrophobic tails of the molecules.

The mixed monolayer with % 10 PEG content does not reveal a significant difference between all subphase conditions as compared in Figure 5.7(b). After expanded phase, there is a slight first order transition between LE and LC states. The surface pressure is increased at approximately the same mean molecular area in the figure, but to a less collapse pressure value. The overall picture says that the 9:1 mixed monolayers have more condensed and packed structures (Figure 5.6) since its isotherms in all subphase solutions are more shifted to a lower mean molecular area then the 8:2 mixed one.

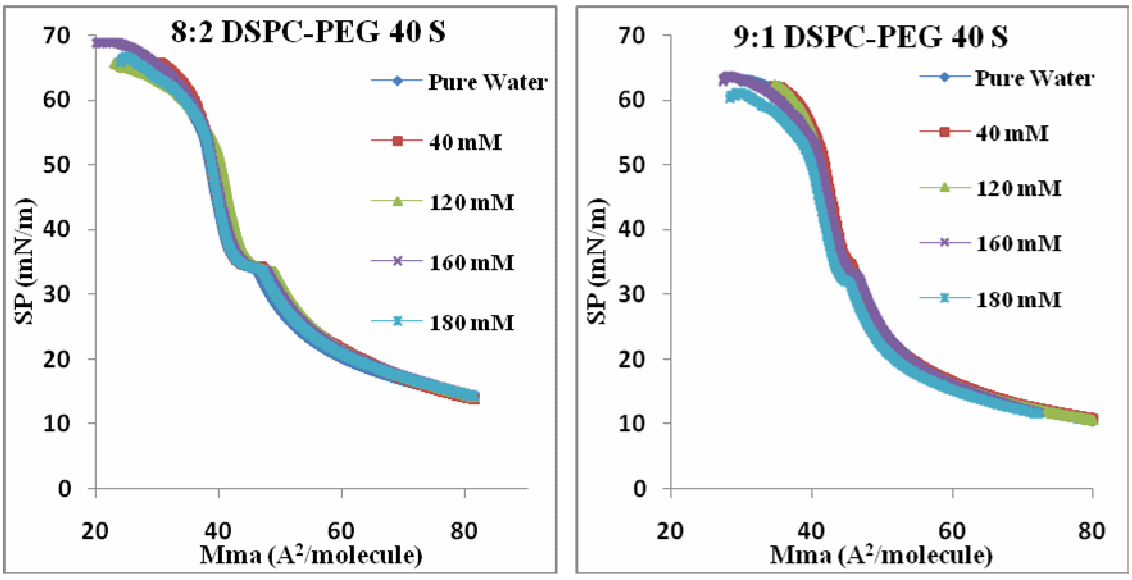

Figure 5.7. The isotherms of (a) 8:2 and (b) 9:1 mixed monolayers on pure water and phosphate buffer solutions at different salt I.S.

The addition of salt into the subphase of the Langmuir trough results in higher total ionic strength values like 160 mM. Also, in order to investigate the effect of different salts on the monolayer films, NaCl and $MgCl_2$ salts were used as the subphase with 180 mM ionic strength. The related isotherms of 8:2 mixed monolayers are shown in Figure 5.6(d) and (e). First of all, like the other 8:2 mixed monolayers, the phase transition is again observed between 40 and 60 A^2 per molecule. The starting point of them is the same; the gaseous (G) phase is not observed. After the expanded phase, around 34 A^2 per molecule, the distinct feature of 8:2 mixed ones are seen as the plateau regions. The surface pressure is increased abruptly in the isotherm showing the liquid condensed phase. At liquid condensed phase, the molecules are in the two-dimensional state since the movement of the molecules is decreased and forms a more ordered structure.

There is also a difference in the mixed monolayers of the 9:1 DSPC-PEG 40 S monolayers. This difference is more clear with the comparison of both mixtures and pure molecules (Figure 5.6). The 9:1 mixture isotherms begin with the expanded phases like the 8:2 mixed ones but to less mean molecular area values. The presence of a small plateau region, a first-order transtion state between LE and LC phases, is observed in the 9:1 mixed monolayers under the buffer effect.

5.2.2. BAM Images

The BAM images of the 8:2 DSPC-PEG 40 S mixed monolayer at the air/water interface are illustrated in Figure 5.8. There is not a distinct feature observed before the plateau region below 34 mN/m surface pressure. These dark phases indicate the expanded phase monolayer properties and this result is consistent with the isothermal graph of 8:2 DSPC-PEG 40 S. In Figure 5.7, the expanded phase regions are seen between 15-34 mN/m surface pressures.

The BAM images of the 8:2 mixed monolayers at the air/water interface begins at around 13 mN/m surface pressure (data not shown here) and represent the similar phase behavior like 15.18 mN/m as depicted in Figure 5.8 (a). The morphological changes of 8:2 mixed monolayers begin at the plateau region. Bright images start to appear and are belong to condensed phase monolayer structure. The condensity is also determined with the bright structures in another study (Arnold et al., 2005). In our study, these bright images increase upon compression and show several condensed structures before the collapse point at about 64 mN/m surface pressure.

The interval between the chosen BAM images is approximately 5 mN/m. Since the camera settings of the BAM measurements have the same parameters, then the different conformations on the surface directly show the effect of the spreading solutions.

Figure 5.9 shows the BAM images of the 9:1 DSPC-PEG 40 S mixed monolayers at the air/water interface. As seen in the isothermal graphs of this mixed monolayer, the condensed phases start to increase between 15 and 20 mN/m surface pressure and continues until reaching the collapse pressure point. There are not phospholipid domain structures on the surfaces. The condensity increases as seen with the bright images and is consistent with the isotherm of the 9:1 mixed monolayer. This mixing molar ratio does not give similar results with the pure components as examined with the 8:2 mixed one. The mixed monolayer of 9:1 DSPC-PEG 40 S behaves more condensed in all surface pressures on the pure water.

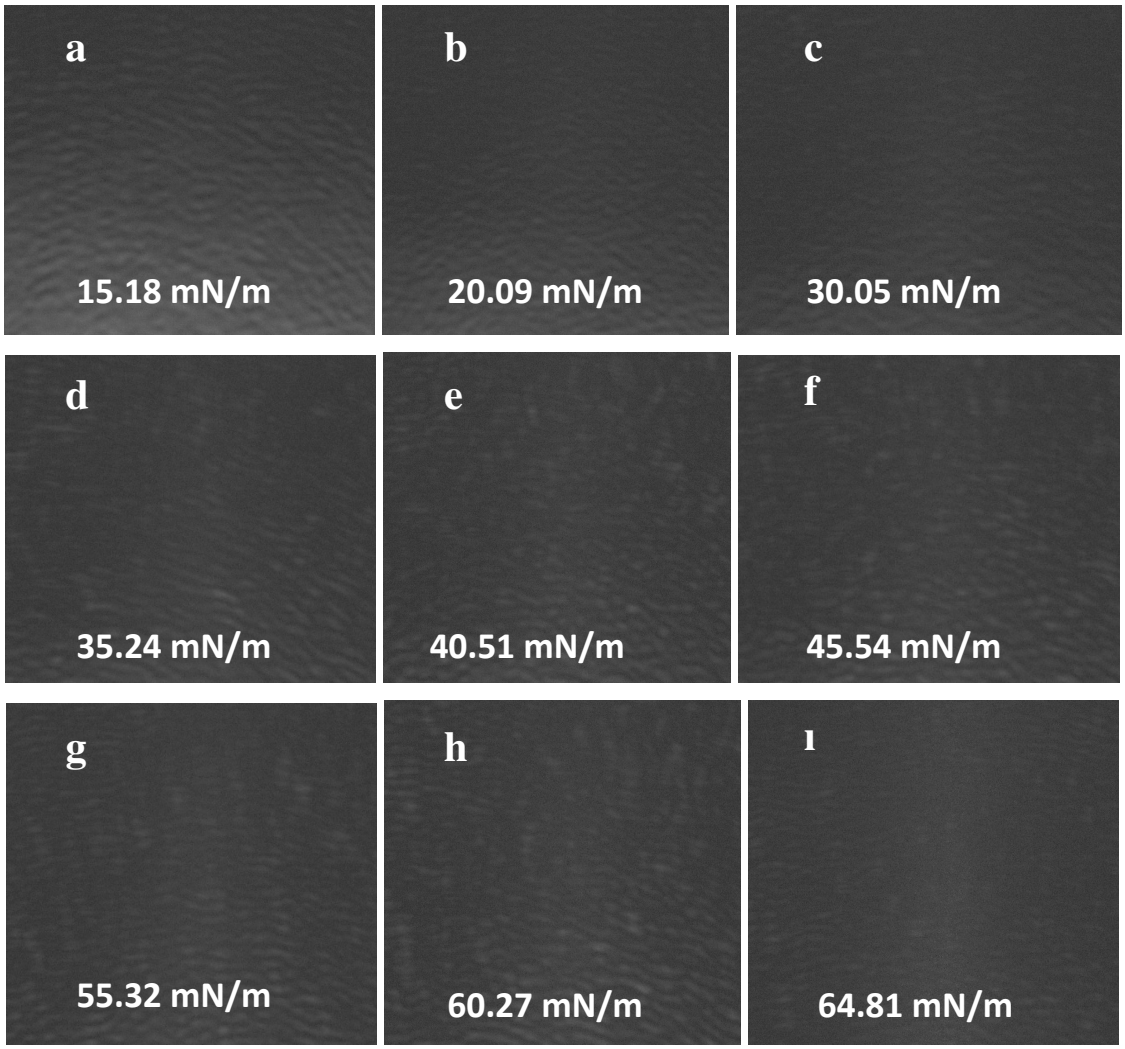

Figure 5.8. The BAM images of the 8:2 DSPC-PEG 40 S mixed monolayers at the air/pure water interface at ambient temperature. The image scale is 400 x 300 μm.

The BAM images of 8:2 DSPC-PEG 40 S mixed monolayers on different buffer solutions are represented in Figure 5.10. Previously, the BAM images of DSPC (Figure 5.5) under different buffer conditions indicate spiral structures when the ionic strength is increased. The mixed monolayers of the 8:2 DSPC-PEG 40 S have also these structures on the subphases when the ionic strength is increased. However, this mixture express different behavior on 180 mM buffer solution. There is not a spiral structure on the subphase. This may be concluded that the $MgCl_2$ salt might have a condensing effect on the monolayer formation.

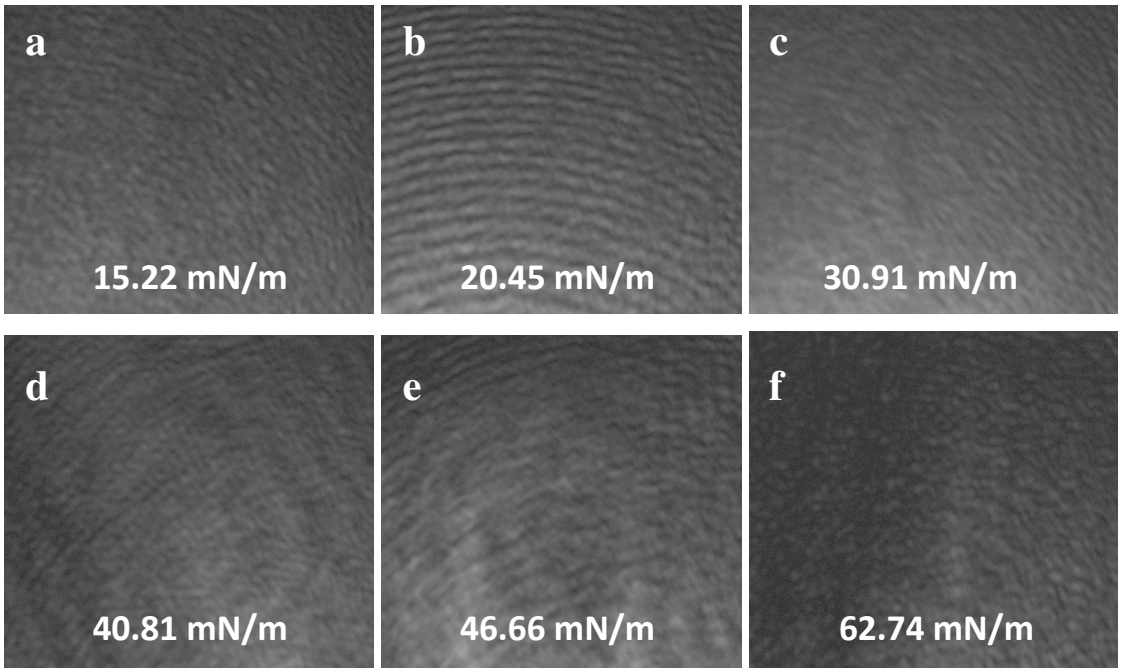

Figure 5.9. The BAM images of the 9:1 DSPC-PEG 40 mixed monolayers at the air/pure water interface at ambient temperature. The image scale is 400 x 300 μm.

At the beginning of the compression about 15 mN/m surface pressure, the mixed monolayer is in the expanded state on the subphase containing 160 mM ionic strength, as it can be seen in the isotherm of this mixture, because the BAM data obtained at that region is a dark image. In the plateau region around 30-35 mN/m surface pressure, bright images begin to appear indicating that the monolayer is in the condensed state. It is consistent with the isotherm data in Figure 5.6(d). Further compression results in spiral shapes on the surface, and destroys the smooth conformation of the condensed phases. The spiral formation with the compression continues until the mixed monolayer collapses at about 69 mN/m surface pressure.

When this situation is compared with the experiment done with pure water, then it can be seen that there is a significant difference between them. The water based one have more dark images than the buffer solution, although several bright images obtained upon compression on water subphase.

The same mixed monolayers under the effect of both NaCl and $MgCl_2$ salts show expanded monolayer structure through the compression with the dark images in 180 mM buffer solution. There is not a distinct feature such as domain formation on the

monolayer. At the plateau region, there is a smooth conformation around 30-35 mN/m surface pressure.

The phase transition at the plateau region between LE and LC phases results in very small bright images at about 45 mN/m surface pressure and are belong to the condensed phase monolayer structure. The collapse pressure point around 66 mN/m surface pressure is consistent with isothermal data of 8:2 DSPC-PEG 40 S under the same buffer condition.

In adddition to these analysis, 9:1 DSPC-PEG 40 S mixed monolayers on buffer solutions generally display more bright and condensed structures (Figure 5.11). The formation of the spiral shapes on the monolayers are not so clear. Therefore, it may be concluded that the choline head group of the molecules are not so much affected with this mixing ratio (9:1) when the ionic strength is increased (Heckl et al., 1986).

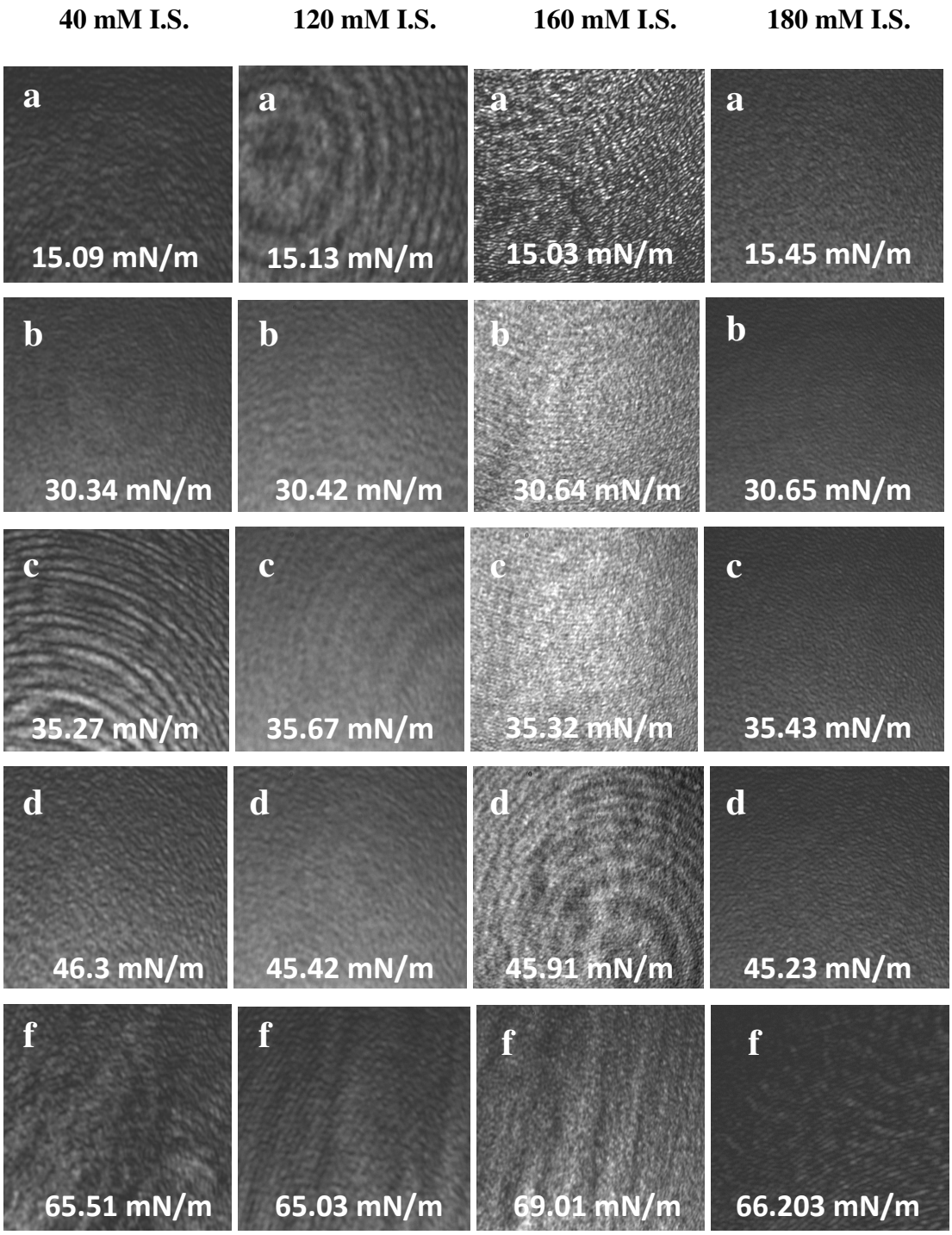

Figure 5.10. The BAM images of the 8:2 DSPC-PEG 40 S mixed monolayers on different buffer conditions at ambient temperature. The image scale is 400 x 300 μm.

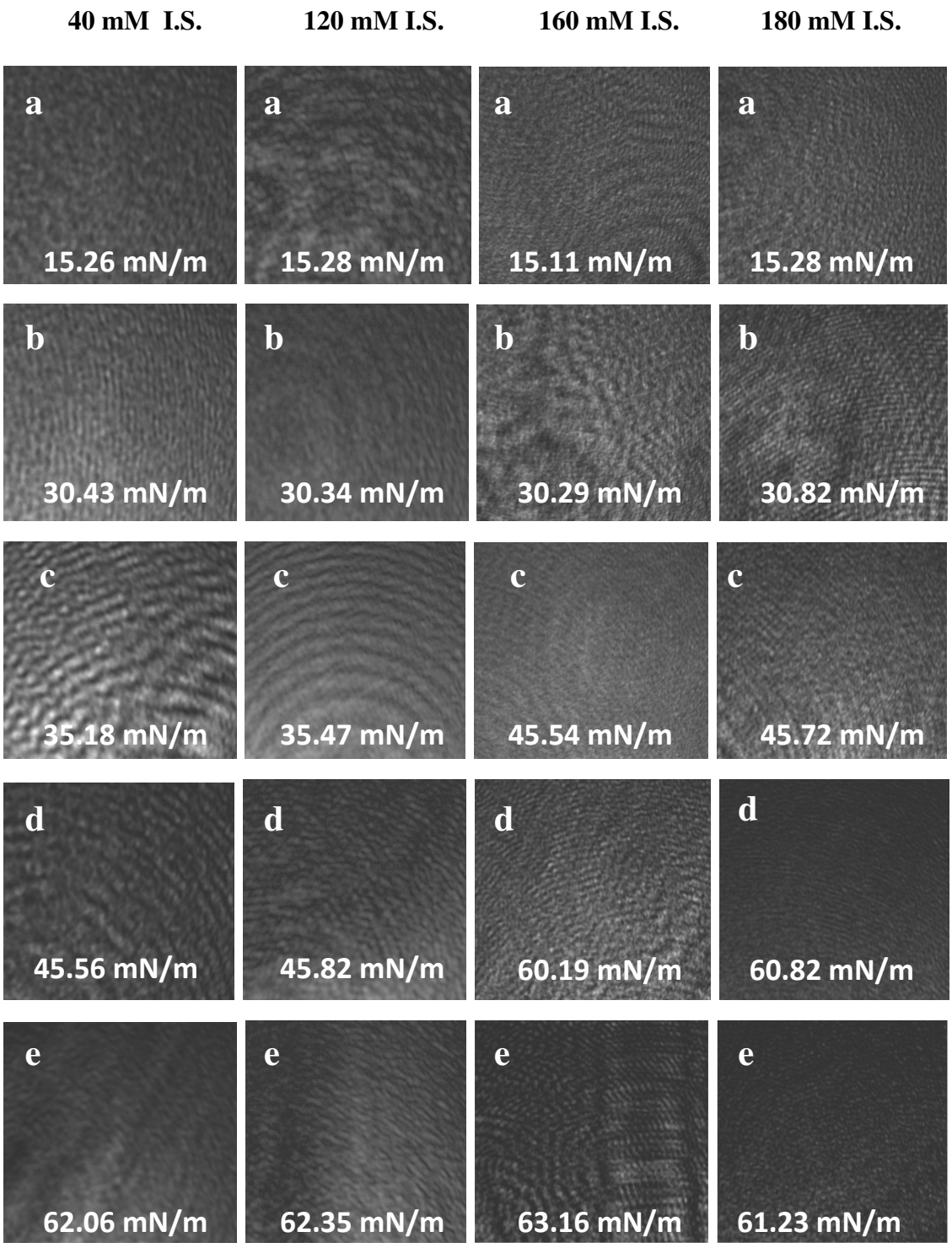

Figure 5.11. The BAM images of the 9:1 DSPC-PEG 40 S mixed monolayers on different buffer conditions at ambient temperature. The image scale is 400 x 300 μm.

5.3. Thermodynamic Stability of Mixed Monolayers

The Lagmuir film can be composed of separate monolayers, if the individual components are immiscible. The sum of the areas of the separate films form the area occupied by the formula given below :

$$A_{ideal} = X_1 . A_1 + X_2 . A_2 \quad (5.1)$$

In this formula, A_{ideal} is the average molecular area of the ideal mixture at a given surface pressure. X_1 and X_2 are the mole fractions of the components; A_1 and A_2 are the molecular areas of the individual components at the same surface pressure values (Petty, 1996). This is the situation for an ideal mixed film. There is a very big difference between an ideal mixed monolayer and the immiscible mixed one. All the intermolecular forces acting on the monolayer are equal in the ideal situation. However, the interactions between molecules in immiscible mixed monolayer differ because of the attractive forces on the film (Gong et al., 2002; Korchowiec et al., 2006).

In the investigation of the miscibility behaviors of the 8:2 and 9:1 DSPC-PEG 40 S mixed monolayers at different subphases, their A_{ex} values were calculated by using the formula:

$$A_{ex} = A_{12} - (X_1 . A_1 + X_2 . A_2) \quad (5.2)$$

Here, Aex indicates the molecular area differences between the ideal mixture and the measured values. Aex is determined by the intermolecular forces between the molecules in a monolayer. Actually, if attractive forces are dominated on the film, then Aex will be negative (Gong et al., 2002).

In Figure 5.12 and 5.13, comparison of the ideal and real mixture situations of the 9:1 and 8:2 mixtures are displayed. According to these analysis, 9:1 mixed monolayers are more near to ideal mixture situation.

In order to compare the real and ideal mixed monolayers, calculations were done with the equation 5.1. As explained previously, X_1 and X_2 were the mole fractions of

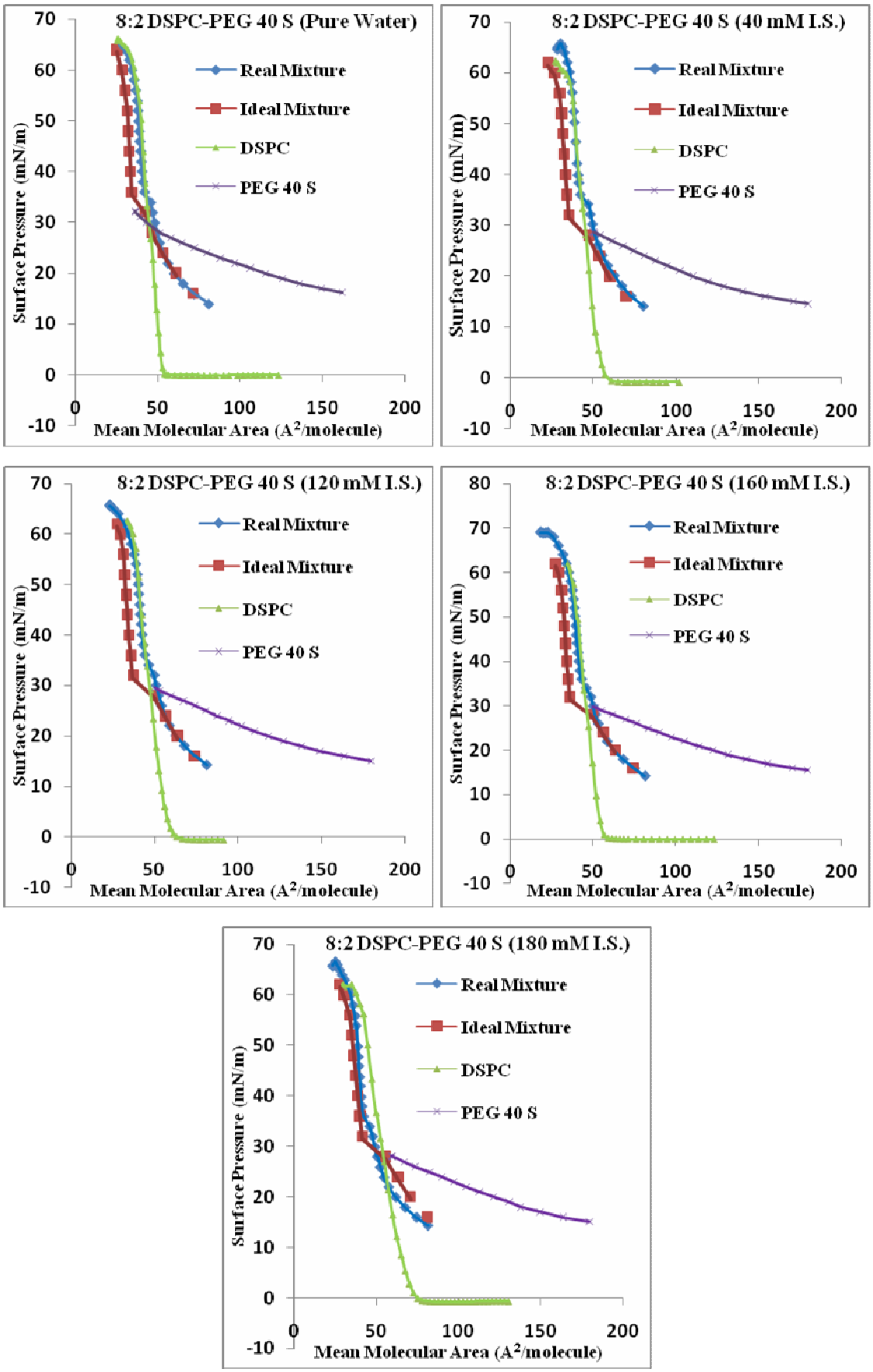

Figure 5.12. Comparison of the ideal and real mixtures of the 8:2 composition.

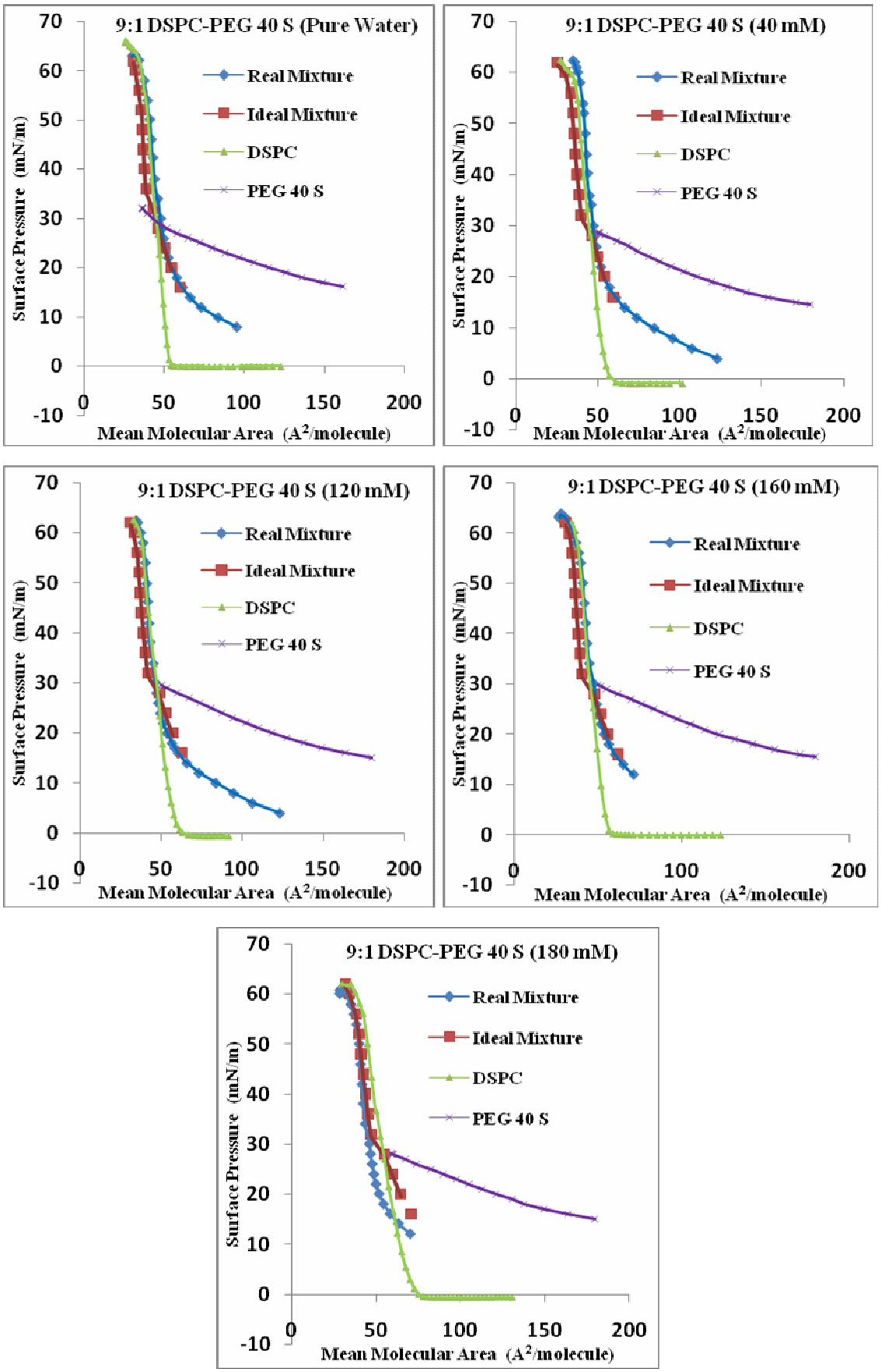

Figure 5.13. Comparison of the ideal and real mixtures of the 9:1 composition.

the mixtures. For example, for the 8:2 mixed monolayers these mole fractions were 0.8 and 0.2 for DSPC and PEG 40 S, respectively.

The mean molecular area of these pure molecules from pure water to buffer media were used in the calculations. However, since PEG 40 S did not reach the high surface pressure values, approximately above 28-29 mN/m surface pressure, the mean molecular area of PEG 40 S kept zero in the formula for the calculations, only the molecular area of the DSPC was used.

The excess free energy of the mixed monolayers can be find out with ΔGex values. At constant surface pressure and temperature in a two-component system, ΔGex is evaluated by this formula:

$$\Delta G_{ex} = \int [A_{12} - (X_1A_1 + X_2A_2)]\, d\pi \qquad (5.3)$$

In this formula, ΔGex can be find out from the LB isotherms. The attraction results in more negative ΔGex values. The most negative state indicates the greatest thermodynamic stability among other conditions in mixed monolayers (Gong et al., 2002).

Theoretically, since the salt ionic strength alters in each of the mixed monolayer, there are differences between these monolayers. This can also be seen in surface pressure-area isotherms. As explained in the study of Helm et al., these isotherms were related with the temperature and on the charge of the head group of the phospholipid molecules. Therefore, the effect of the ionic strength is directly related with these interactions on the subphase (Helm et al., 1987). The Aex versus total ionic strength calculations were done in order to understand this interaction between the molecules.

In order to detect the impact of the subphase solutions, the thermodynamic analysis of the 8:2 and 9:1 mixtures were evaulated separately like seen in Figure 5.14. In these graphs, when the ionic strength is increased, 9:1 mixture reaches more negative ΔG_{ex} values and indicate the molecular attraction between its molecules.

The thermodynamic stability of the 8:2 DSPC-PEG 40 S mixed monolayers at different ionic strengths at various surface pressures is shown in Figure 5.15. In the figure, 40 mM ionic strength does not give a significant change between molecules because the excess energy values are positive; the molecular interactions are in the repulsive form in all surface pressures.

When the ionic strength is increased, the interactions are increased, too. It can be seen in the graph that the most attractive forces are predominated at 180 mM total ionic strength condition. Therefore, this shows that using $MgCl_2$ and NaCl salts together increase the intermolecular forces between the molecules and this results in more negative ΔG_{ex} values. The graph indicates 28 mN/m surface pressures have the highest negative value. These surface pressures are belong to the expanded phase regions in the 8:2 mixed monolayer isotherm.

The molecular interactions are at the highest point until they reach the plateau region at about 28 mN/m. In the plateau region, molecular interactions are not very active in the buffers containing only NaCl salt. However, after the addition of $MgCl_2$ to the solution, interactions are increased and negative values are seen for both of the mixtures (Figure 5.15). According to the Gouy-Chapman theory, increasing the Na^+ ionic strength from 10^{-4} to 10^{-2} M resulted in the change of the head group from 0.4 e/molecule to 0.9 e/molecule (Helm et al., 1987). Therefore, the high molecular interactions with the addition of both Na^+ and Mg^{+2} ions to the solution as seen in thermodynamic analysis can be explained in the light of this result.

There is an assumption about the two-dimensional phase transitions. For example, transition from an expanded state to a condensed one, Van der Waals forces are thought to be reason for this transition in long-chain fatty acids (Jähnig, 1979; Marcelja, 1974; rewieved in Petty, 1996). According to this theory, since our main phospholipid used in the experiments, is a long-chain one (C18), then the intermolecular forces acting on the expanded phase and giving the most negative ΔG_{ex} values may be Van der Waals forces.

The thermodynamic behaviors of the mixed monolayers of the 9:1 DSPC-PEG 40 S at different surface pressures and ionic strengths are showed also in Figure 5.15. In these graphs, 0 mM refers to the pure water condition. Mixed monolayers on pure water exhibit almost the same molecular interactions at 32 mN/m surface pressure. There is not a significant difference between them. This analysis for 32 mN/m was done only to the pure water condition. ΔG_{ex} calculations for other surface pressures (20, 24 and 28 mN/m) as seen in Figure 5.15 was done for all the subphase solutions so as to investigate the molecular interactions when the surface pressure and also the ionic strength was increased.

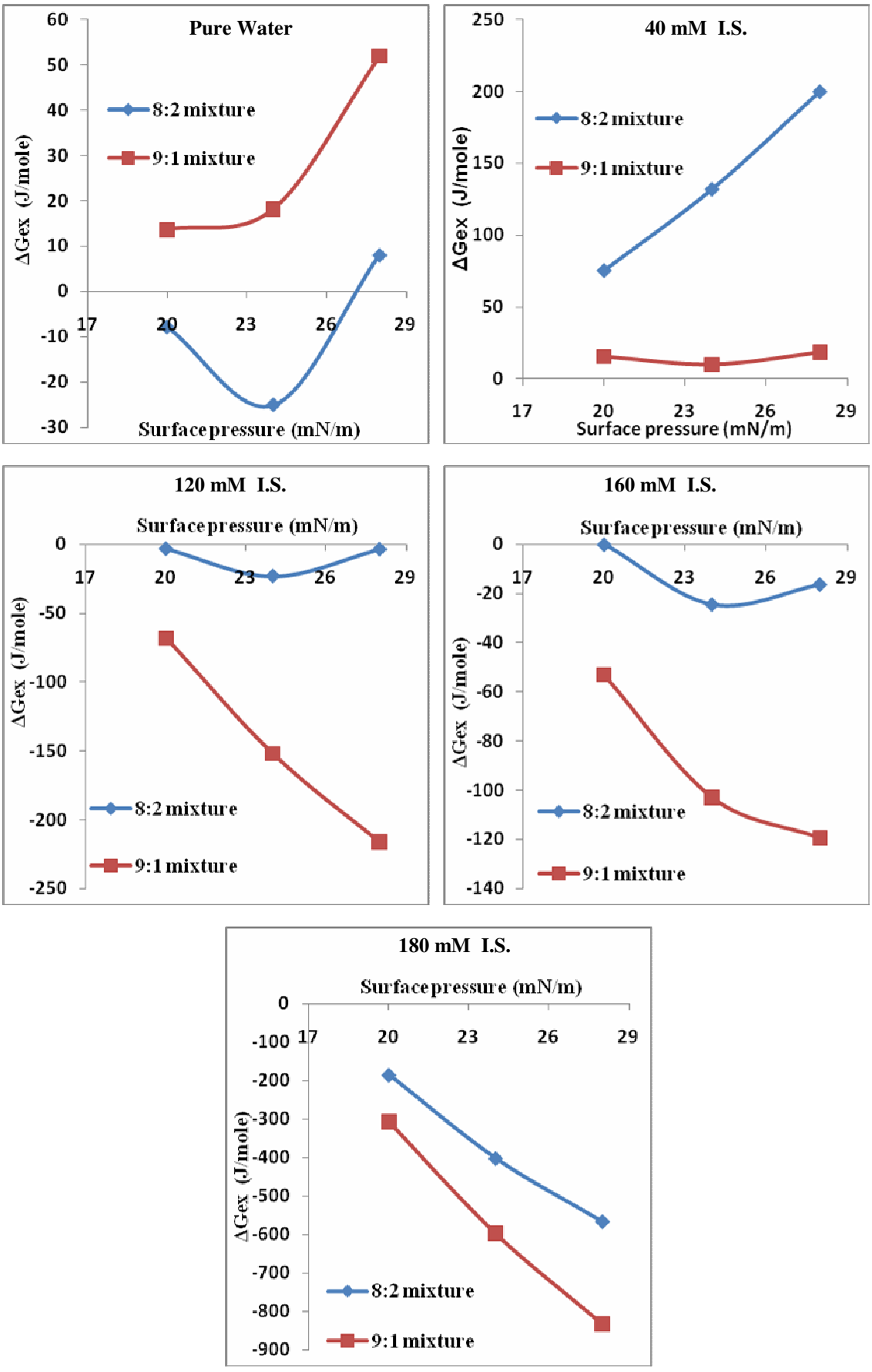

Figure 5.14. ΔGex analysis of the mixed monolayers.

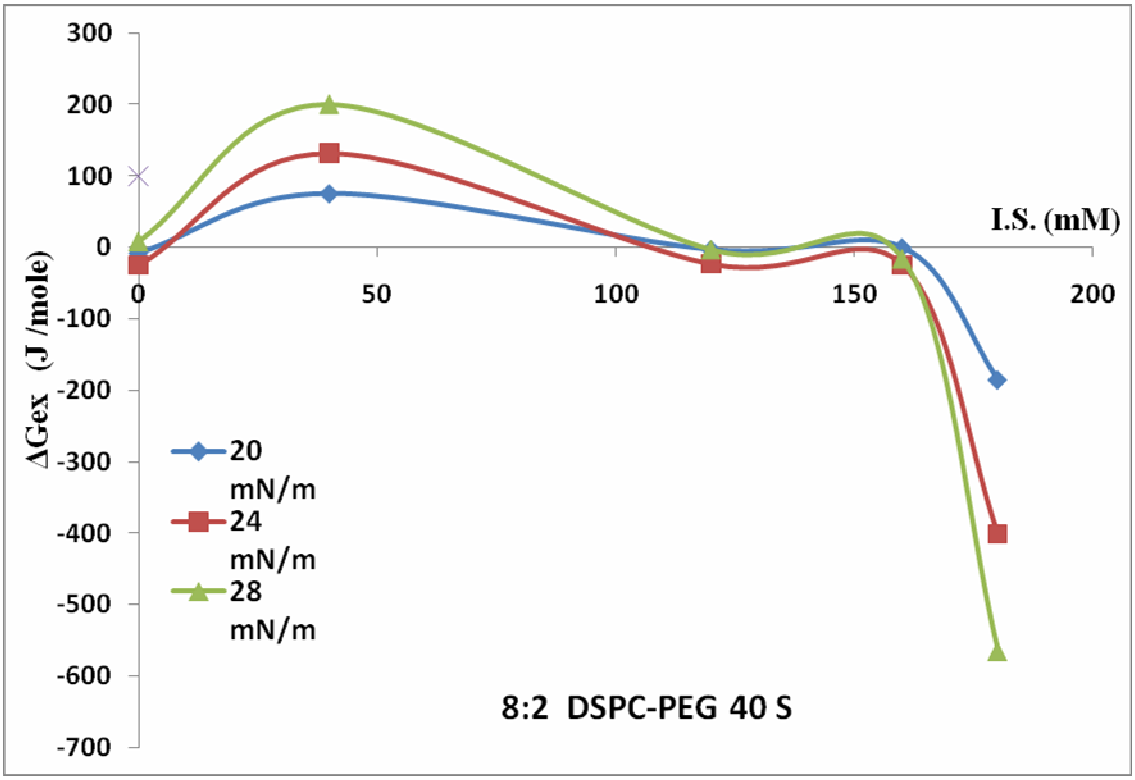

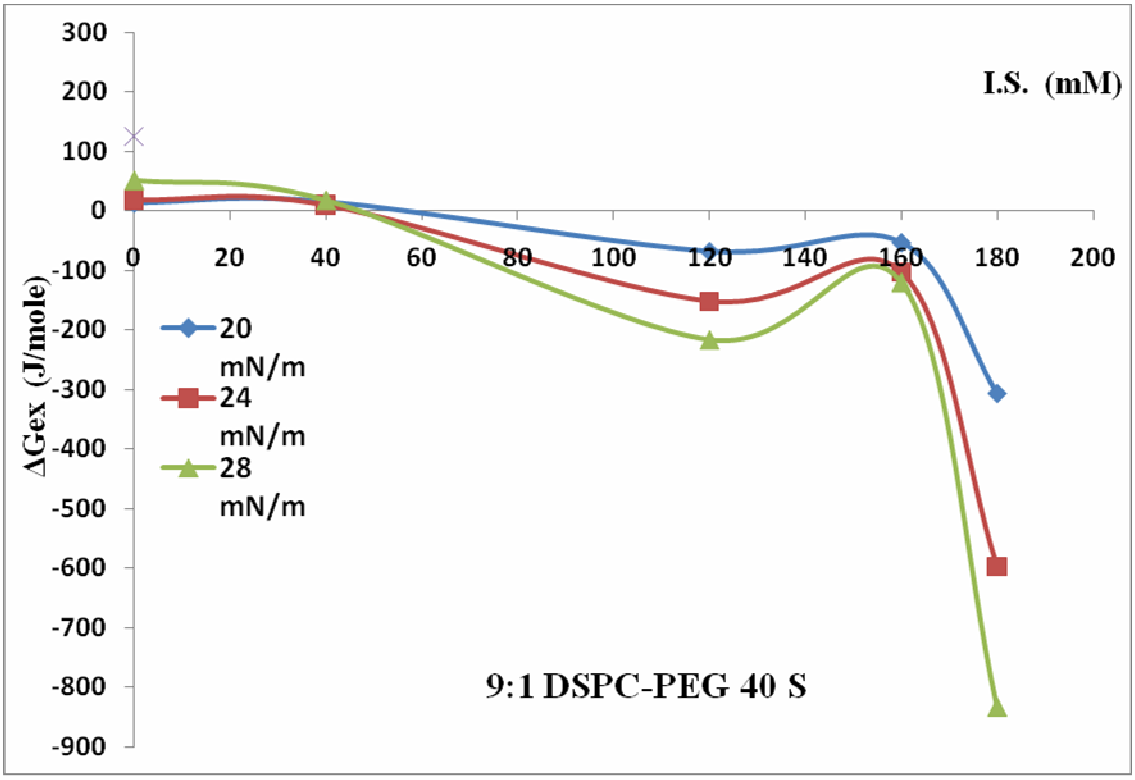

Figure 5.15. The thermodynamic stability of the mixed monolayers on different subphases.

When these analysis are compared with the isothermal graph of the 9:1 mixed monolayers in Figure 5.1(b-e), it can be seen that the attractive forces are predominated especially in the expanded phases at 28 mN/m surface pressure. This consequence is similar with the 8:2 mixed monolayers. Thus, it can be said that the addition of $MgCl_2$ to the NaCl solution increase the attractive forces and also decrease the repulsive forces between the molecules on the subphase. Like the assumption done previously, this increase between molecules can be clarified with the Gouy-Chapman theory. According the study of Helm et al., only increasing the Na^+ ion in the solution resulted in the higher attraction between phospholipid head groups (Helm et al., 1987). Thus, as seen in Figure 5.15, more negative ΔGex values were obtained with the addition of both NaCl and $MgCl_2$ salts to the buffer solutions.

These attractive forces may be the effects of Van der Waals interactions of the molecules, since the DSPC molecule has a long hydrocarbon chain. However, upon further compression, the monolayer goes into a phase transformation and forms a plateau region at around 30 mN/m surface pressure. At this plateau region, repulsive forces are predominated like the evaluation done to the 8:2 mixed monolayers above.

The effect of the surfactant on the miscibility behaviors of these two mixed monolayers indicate that the 9:1 DSPC-PEG 40 S has much more attractive forces with the most negative excess area values. The BAM images of the 9:1 mixed monolayers represent the more condensed structures as seen in Figure 5.11. The head group of the amphiphlic molecules were not so much affected from the increase of the ionic strength and express more smooth surfaces among other images.

The compressibility analysis of the mixed monolayers were also done with the formula (Gong et al., 2002) given below for each of the mixtures under the known buffer conditions.

$$1 / C_s = -A. (d\pi / dA) \qquad (5.4)$$

In this formula, A is the area per molecule for a known surface pressure. $1/C_s$ is the incompressibility parameter and shows the proportion of surface pressure and area. From the raw data of the related π-A isotherms, $1/C_s$ values were calculated. Generally, if the incompressibility factor ($1/C_s$) is greater for the mixed monolayers ,then more condensed films will be obtained (Gong et al., 2002).

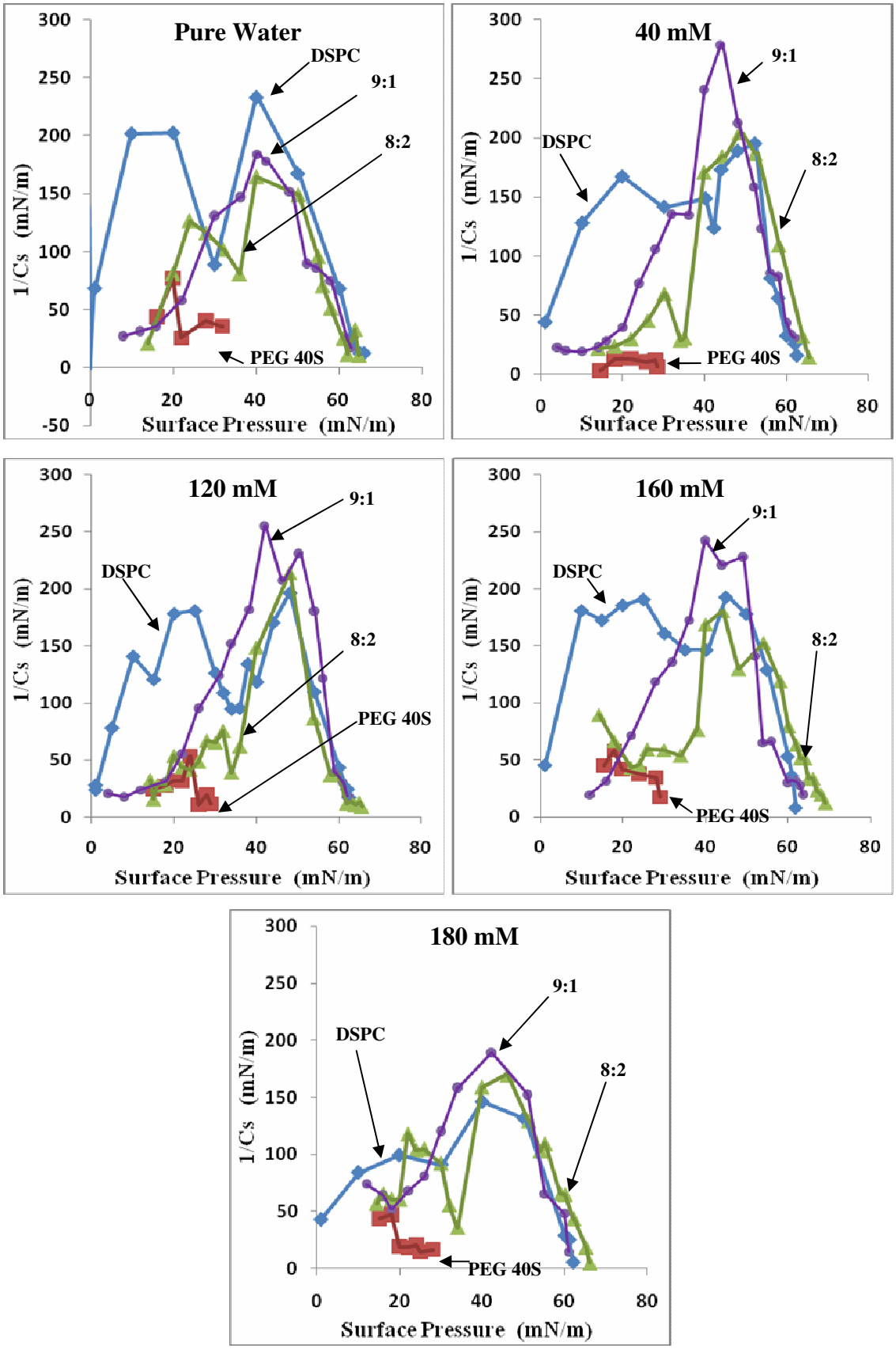

Figure 5.16. Surface compressional modulus (1/Cs) of the mixed monolayers and pure components on different subphases.

In Figure 5.16, incompressiblity analysis of pure molecules and mixed monolayers on different buffer conditions are given separately. In all graphs, there exist several fluctuations. PEG 40 S is more flexible in all conditions, and this is directly related with its bulky structure. In addition to this, DSPC is more flexible when the ionic strength is increased. The flexibility of the DSPC monolayers is increased with the increase of the ionic strength.

The 9:1 mixed monolayers in all buffer solutions display a peak between 40-60 mN/m surface pressure, where the isotherm of them goes condensed state. At this peak point, elasticity of the monolayers decrease and after this increase, 1/Cs values decrease suddenly and reaches the point of their collapse pressure.

The peak point of the 8:2 mixed monolayers is not very clear on the graphs like the other mixture. However, it can be seen that the 9:1 mixture reaches higher incompressibility values and display more condensed structures in all conditions.

The incompressibility analysis of 8:2 and 9:1 mixed monolayers in Figure 5.17 shows that the monolayers with 9:1 mixing ratio are display less fluctuations under all subphase conditions then the other mixture.

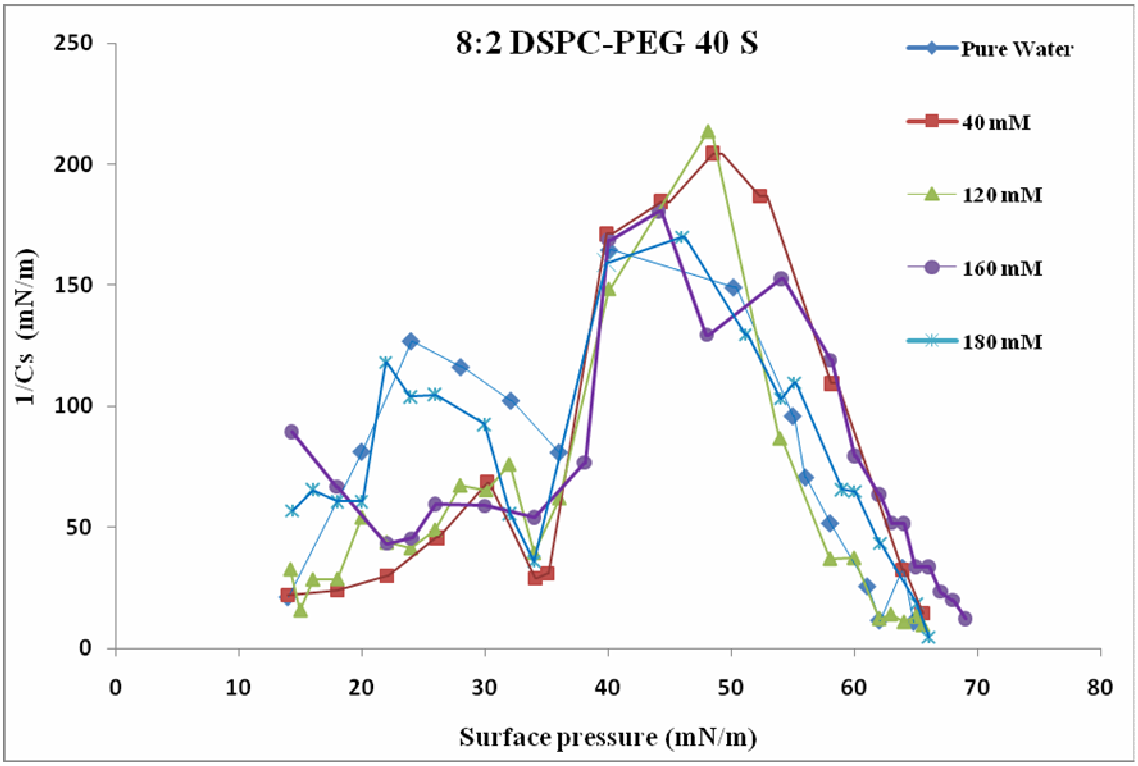

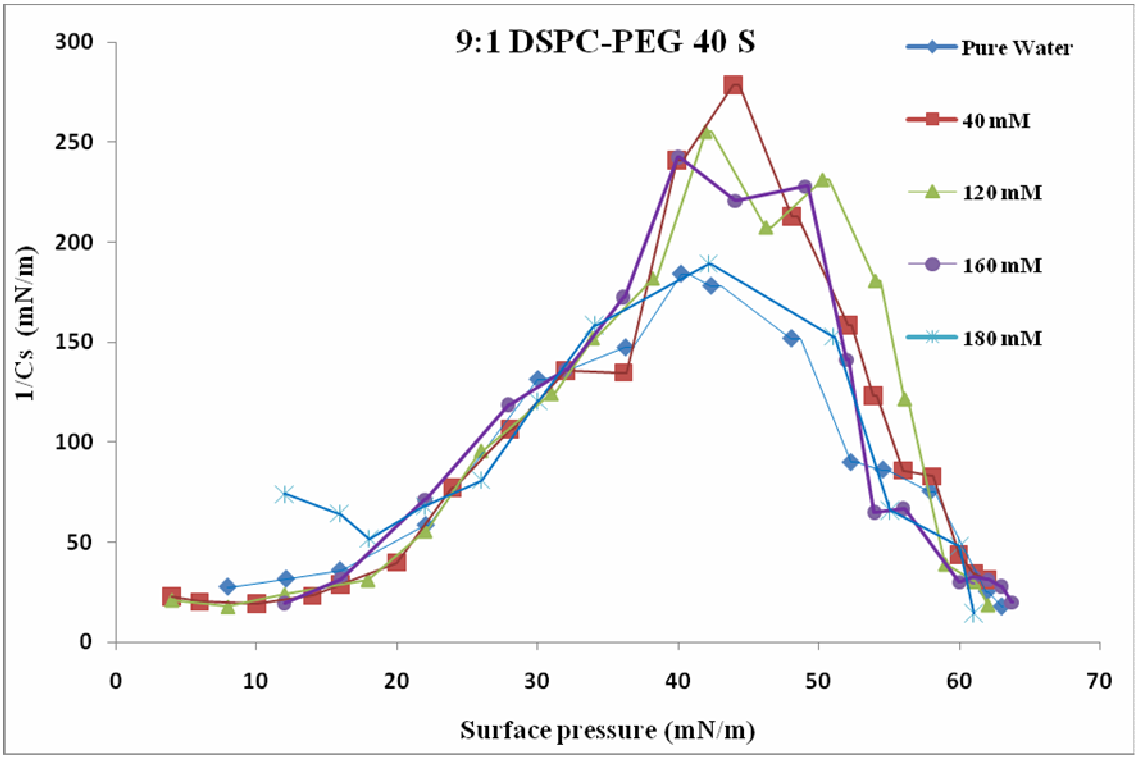

Figure 5.17. Surface compressional modulus(1/Cs) of the 8:2 and 9:1 DSPC-PEG 40 S mixed monolayers on different subphases.

CHAPTER 6

CONCLUSION

In this thesis work, monolayer formation of the emulsifier and the phospholipid molecules were investigated by LB and BAM techniques on the air/water and also on the phosphate buffer interfaces. The subphases used in the Langmuir troughs contained different ionic strength values.

The goal of this study is to find out the more appropriate subphase and mixture composition for the bubble formation. In the literature, there is not a composition with the molar ratio of 8:2 phopholipid-emulsifier ratio in the bubble production. In our study, we tried this ratio whether it is more suitable to obtain more stable microbubbles, or not, and compare the results with the commonly used molar ratio (9:1).

The molecular interactions between the pure molecules and the mixed monolayers which were indicated by 8:2 and 9:1 DSPC-PEG 40 S, showed distinct features both in LB and BAM techniques. According to the quantitative analysis of the mixed monolayers, it was observed that 9:1 mixture on the subphase had more attractive forces between their molecules than the other mixture. More negative ΔG_{ex} values were obtained from the 9:1 DSPC-PEG 40 S mixture. Higher ionic strength conditions displayed more condensed monolayer features for the 9.1 mixture. The 180 mM buffer condition expressed higher attraction between the molecules and the subphase.

It was intended to obtain a stable and homogeneous monolayer structure on the surface of the microbubbles, and this aim is consistent with the data obtained from LB and BAM analysis.

The condensity behavior of the monolayers is very important for the production of the micron-sized bubbles for ultrasound imaging in medical diagnosis. Therefore, 9:1 mixture composition display more condensed monolayer formation with higher 1/Cs values on all the subphases.

The experiments and analysis done in this study were the first step of the investigation of the shell structure of ultrasound contrast agents as microbubbles. Microbubble production and development will be carried out in the light of these investigations.

REFERENCES

Arnold, A.; Cloutier I.; Ritcey, A. M.; Auger, M., '*Temperature and Pressure Dependent Growth and Morphology of DMPC/DSPC Domains Studied By Brewster Angle Microscopy*', Chemistry and Physics of Lipids 133, 165-179, 2005.

Barlow D. J.; Hollinshead C. M. ; Harvey R. D.; Kudsiova L.; Lawrence M. J., '*Memory effects of monolayers and vesicles formed by the non-ionic surfactant, $2C_{18}E_{12}$*' , Journal of Colloid and Interface Science, 316, 741-750, 2007.

Basnet, P, B, '*Patterns and Conformations in Molecularly Thin Films*', Doctoral Thesis, May 2010.

Borden, M. A. and Longo M. L., '*Dissolution Behavior of Lipid Monolayer-Coated, Air-Filled Microbubbles: Effect of Lipid Hydrophobic Chain Length*', Langmuir, Vol. 18, No. 24, 2002.

Borden, M. A.; Pu, G.; Runner G. J.; Longo M. L., '*Surface phase behavior and microstructure of lipid/PEG-emulsifier monolayer-coated microbubbles*', Colloids and Surfaces B: Biointerfaces 35, 209-223, 2004.

Borden, M. A.; Kruse, D. E.; Caskey, C. F.; Zhao, S.; Dayton, P. A.; Ferrara, K. W., '*Influence of Lipid Shell Physicochemical Properties on Ultrasound-Induced Microbubble Destruction*', IEEE Trans Ultrason Ferroelectr Freq. Control., Vol. 52, No.11, 2005.

Borden, M.; '*Nanostructural features on stable microbubbles*', Soft Matter, 5, 716-720, 2009.

Chatterji, D. and Rajdev, P., '*Macromolecular recognition at the air–water interface: application of Langmuir–Blodgett technique*', CURRENT SCIENCE, Vol. 95, NO. 9, 2008.

Chlon, C.; Guedon, C.; Verhaagen, B.; Shi, W. T.; Hall, C. S.; Lub, Böhmer, M. R., '*Effect of Molecular Weight, Crystallinity, and Hydrophobicity on the Acoustic Activation of Polymer-Shelled Ultrasound Contrast Agents',* Biomacromolecules, 10, 1025–1031, 2009.

Degen, P., Rehage, H., Klärner, F. and Polkowska, J. '*Characterization of Langmuir monolayers of molecular clips by means of Brewster angle microscopy*', Colloid and Polymer Science. 2005. 284:44-50.

DeWolf, C.; Leporatti, S.; Kirsh, C.; Klinger, R.; Brezesinski, G. '*Phase separation in phosphatidylinositol/phosphatidylcholine mixed monolayers*', Chemistry and Physics of Lipids, 97, 129-138, 1999.

Dijkmans, P. A.; Juffermans, L. J. M.; Musters, R. J. P.; Wamel, A. Van; ten Cate, F. J.; Gilst, W. van; Visser, C. A.; Jong, N. de; Kamp, O., 'Microbubbles and ultrasound: from diagnosis to therapy' , Eur J Echocardiography 5, 245-256, 2004.

Ferrara K. W.; Borden, M. A.; Dayton, P.; Zhao, S., '*Physico-chemical Properties of The Microbubble Lipid Shell*', IEEE Ultrasonics Symposium, 2004.

Gong, K.; Feng, S.; Go, M. L.; Soew, P. H., '*Effects of pH on the stability and* compr*essibiliy of DPPC / cholesterol monolayers at the air-water interface*', Colloids and Surfaces A: Physicochemical and Engineering Aspects, 207, 113-125, 2002.

Gramiak R.; Shah, P. M., '*Echocardiagraphy of the aortic root*', Invest. Radiol. 3, 356, 1968.

Hecht, E. '*Optics*', International Edition, Addison Wesley, 2002.

Heckl, W. M.; Lösche, M.; Cadenhead, D. A.; Möhwald, H., '*Electrostatically induced growth of spiral domains in the presence of cholesterol*', Eur. Biophys. J. 14, 11-17, 1986.

Helm, C. A.; Möhwald, H.; Kjaer, K.; Als-Nielsen, J., '*Phospholipid Monolayers Between Fluid and Solid States*', Biophysics J., Vol. 52, 381-390, 1987.

Hollinshead, C. M.; Harvey, R. D.; Barlow, D. J.; Webster, J. R. P.; Hughes, A. V.; Weston, A.; Lawrence,M.J, '*Effects of Surface Pressure on the Structure of Distearoylphosphatidylcholine Monolayers Formed at the Air/Water Interface*', Langmuir, 25, 4070-4077, 2009.

Jähnig, F., '*Molecular theory of lipid membrane order*', J. Chem. Phys., 70, 3279-90, 1979.

KSV Langmuir and Langmuir-Blodgett (LB) Films Manual.

KSV Optrel, *Brewster Angle Microscopy* (BAM) 300 Manual, (KSV Instruments Ltd.).

Klibanov, A. L., 'Book Chapter: *Molecular Imaging with Targeted Ultrasound Contrast Microbubbles', 'Molecular Imaging-An Essential Tool in Preclinical Research*, *Diagnostic Imaging,and Therapy*', Springer, 2005.

Korchowiec, B.; Paluch, M.; Corvis, Y.; Rogalska, E., '*A Langmuir film approach to elucidating interactions in lipid membranes: 1,2-dipalmitoyl-sn-glycero-3-phospho ethanola- mine / cholesterol / metal / cation systems*', Chemistry and Physics of Lipids, 144, 127-136, 2006.

Kubo, I.; Adachi, S.; Maeda, H.; Seki, A., '*Phosphatidylcholine monolayers observed with Brewster angle microscopy and π-A isotherms*', Thin Solid Films, 393, 80-85, 2001.

Lawrie, G. A.; Gentle, I. R.; Barnes, G. T., '*The structure of mixed monolayer films of DPPC and hexadecanol*', Colloids Surfaces A, 171, 217-224, 2000.

Li, J. B.; Miller, R.; Volhart, D.; Möhwald, H., '*Spreading Concentration Effect on the Morphology of Phospholipid Monolayers*', Thin Solid Films, 327-329, 84-86, 1998.

Liang H-D; Blomley, M. J.; '*The role of ultrasound in molecular imaging*', The British Journal of Radiology, Special Issue 2003.

Lucero, A.; Rodríguez Nino, M. R.; Gunning, A. P.; Morris, V. J.; Wilde, P. J.; Rodríguez Patino, J. M. '*Effect of Hydrocarbon Chain and pH on Structural and Topographical Characteristics of Phospholipid Monolayers*', J.Phys. Chem. B, 112, 7651-7661, 2008.

Ma, G. and Allen, H. '*DPPC Langmuir monolayer at the air-water interface: Probing the tail and head groups by vibrational sum frequency generation spectroscopy*', Langmuir, 22:5341-5349, 2006.

Marcelja, S., '*Chain ordering in liquid crystals II. Structures of bilayer membranes'*, Biochem. Biophys. Acta., 367, 165-76, 1974.

Meunier, J. '*Why a Brewster angle microscope?*' Colloids and Surfaces A: Physicochemical and Engineering Aspects, 171:33-40, 2000.

Moghaddam, B.; Ali, M. H. ; Wilkhu, J.; Kirby, D. J.; Mohammed, A. R.; Zheng, Q.; Perrie, Y., '*The application of monolayer studies in the understanding of liposomal formulations*', International Journal of Pharmaceutics, xxx, xxx-xxx, 2011.

Unger, E. C.; Porter, T.; Culp, W.; Labell, R.; Matsunaga, T.; Zutshi, R.; '*Therapetic applications of lipid coated microbubbles*', Advenced Drug Delivery Reviews, 1291-1314, 2004.

Optrel GBR, *Brewster Angle Microscopy* (BAM) Manual.

Petty, M. C., '*Langmuir-Blodgett Films-An introduction*', (Cambridge University Press, Cambridge), pp. 25-37,1996.

Pu, G.; Borden, M. A.; Longo, M.,'*Collapse and Shedding Transitions in Binary Lipid Monolayers Coating Microbubbles*', Langmuir, 22, 2 993-2999, 2006.

Riess, J. G.; Schutt, E. G.; Klein, D. H.; Mattrey, R. M.; '*Injectable microbubbles as Contrast Agents for Diagnostic Ultrasound Imaging. The Key Role of Perfluorochemicals*', Angew. Chem. Int. Ed., 42, 3218-3235, 2003.

Sboros, V.; Tang, M-X, '*The assessment of microvascular flow and tissue perfusion using ultrasound imaging*', Proceedings of the Institution of Mechanical Engineers, Part H: Journal of Engineering in Medicine 224: 273, 2010.

Sirsi, S.; Borden, M., *'Microbubble Compositions, Properties and BiomedicalApplications',* Bubble Sci. Eng Technol., 1(1-2): 3–17, 2009.

Stride, E.; Edirisinghe, M., '*Novel microbubble preparation technologies*', Soft Matter, 4, 2350-2359, 2008.

Wang, W.; Moser, C.; Wheatley, M. A., 'Langmuir Trough Study of Surfactant Mixtures used in the production of a New Ultrasound Contrast Agent Consisting of Stabilized Microbubbles', J. Phys. Chem., 100 (32), 13815-13821, 1996.

Zasadzinski, J. A.; Viswanathan, R.; Madsen, J. G; Schwartz D. K., '*Langmuir-Blodgett Films*', Science, Vol. 263, 1994.